

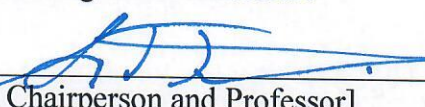
AMERICAN UNIVERSITY OF BEIRUT

HEPARIN-MIMETIC ALGINATE
SULFATE/POLYCAPROLACTONE DOUBLE EMULSION
NANOPARTICLES FOR ENHANCED INSULIN-LIKE GROWTH
FACTOR (IGF-1) DELIVERY AND DIABETIC WOUND HEALING
APPLICATIONS

by
DUAA BASSAM FAHS

Approved by:

[Dr. Rami Mhanna, Assistant Professor] Advisor
[Biomedical Engineering Program]
Maroun Semaan Faculty of Engineering and Architecture


[Dr. Ayad Jaffa, Assistant Dean, Chairperson and Professor] Co-advisor
[Department of Biochemistry and Molecular Genetics]
Faculty of Medicine

[Dr. Ali Tehrani, Associate Professor] Member of Committee
[Bahaa and Walid Bassatne Department of Chemical Engineering and Advanced Energy]
Maroun Semaan Faculty of Engineering and Architecture

[Dr. Firas Kobaissy, Visiting Associate Professor] Member of Committee
[Department of Biochemistry and Molecular Genetics]
Faculty of Medicine

Date of thesis/dissertation defense: [January 26, 2021]

AMERICAN UNIVERSITY OF BEIRUT

HEPARIN-MIMETIC ALGINATE
SULFATE/POLYCAPROLACTONE DOUBLE EMULSION
NANOPARTICLES FOR ENHANCED INSULIN-LIKE
GROWTH FACTOR (IGF-1) DELIVERY AND DIABETIC
WOUND HEALING APPLICATIONS

by
DUAA BASSAM FAHS

A thesis
submitted in partial fulfillment of the requirements
for the degree of Master of Science
to the Biomedical Engineering Program
of the Maroun Semaan Faculty of Engineering and Architecture
and the Faculty of Medicine
at the American University of Beirut

Beirut, Lebanon
January 2021

AMERICAN UNIVERSITY OF BEIRUT

THESIS RELEASE FORM

Student Name: Fahs Duaa Bassam
 Last First Middle

I authorize the American University of Beirut, to: (a) reproduce hard or electronic copies of my thesis; (b) include such copies in the archives and digital repositories of the University; and (c) make freely available such copies to third parties for research or educational purposes:

- As of the date of submission
- One year from the date of submission of my thesis.
- Two years from the date of submission of my thesis.
- Three years from the date of submission of my thesis.

 Duaa Fahs February 6, 2021

Signature

Date

ACKNOWLEDGEMENTS

In the Name of Allah, the Most Beneficent, the Most Merciful.

First and most importantly, I would like to thank Allah (swt) for all his blessings, without his guidance I would not be where I am today.

I would like to express the deepest gratitude and appreciation to my advisor, Dr. Rami Mhanna, for his direction, guidance, support, as well as encouragement in helping me become the independent thinker I am today.

It is with immense thankfulness that I acknowledge the guidance of my co-advisor Dr. Ayad Jaffa, and most importantly for giving me the chance to work in his lab.

A word of appreciation goes out to Mia Karam, my friend and research mentor, for her day-to-day support and help throughout every single step of this journey, and for teaching me the laboratory techniques that I performed for my thesis work.

I would like to thank Batoul Maatouk for helping me whenever I was in need. I also thank Maryam Baydoun for making the Lab a positive environment.

I would like to thank my committee members Dr. Ali Tehrani and Dr. Firas Kobaissy for serving as committee members for this thesis.

Finally, nobody has been more important to me on the journey of this project than the members of my family and close friends. I would like to dedicate this thesis to my parents who have given me the opportunity of an education from the best institutions and support throughout my life.

ABSTRACT OF THE THESIS

Duaa Bassam Fahs

for

Master of Science

Major: Biomedical Engineering

Title: Heparin-mimetic Alginate Sulfate/Polycaprolactone Double Emulsion Nanoparticles for Enhanced Insulin-like Growth Factor (IGF-1) Delivery and Diabetic Wound Healing Applications

Introduction: Diabetic foot ulcers (DFUs) are a complication to diabetes mellitus that cause 85% of all amputations worldwide and pose an annual economic burden of \$15 billion. The wound healing process is altered in DFU patients partly due to the deficiency of growth factors (GF) such as insulin-like growth factor-1 (IGF-1). To address the problem of GF deficiency in DFU, we engineered double emulsion nanoparticles (NPs) using heparin-mimetic alginate sulfate (AlgSulf) for the encapsulation and sustained release of IGF-1 to promote wound repair and decrease inflammation in the wound microenvironment.

Methods: NPs were synthesized with an AlgSulf core and polycaprolactone (PCL) shell via the solvent evaporation technique. The NPs were characterized for their size, zeta potential, and polydispersity index using dynamic light scattering, and morphology using scanning electron microscopy. IGF-1 encapsulation efficiency (EE) and release rate were analyzed using enzyme-linked immunosorbent assay (ELISA). The NPs' cytotoxicity was assessed on human keratinocyte (HaCaT) cell line using trypan blue and MTT assays. Cellular uptake of the NPs was evaluated by assessing the fluorescence intensity of HaCaT cells treated with fluorescently labeled Alg or AlgSulf loaded NPs. The ability of NPs to reduce inflammation was measured by quantifying the mRNA and protein expression levels of IL-6 inflammatory marker using qRT-PCR and ELISA.

Results: NPs with AlgSulf of a degree of sulfation (DS=2) AlgSulf2.0/PCL had the smallest average size and lowest zeta potential ($p < 0.05$). IGF-1 EE was higher in AlgSulf NPs compared to non-sulfated Alg-based NPs ($98.59\% \pm 0.48$ and $97.43\% \pm 2.83$ AlgSulf0.8/PCL and AlgSulf2.0/PCL NPs, respectively compared to $95.56\% \pm 1.89$ for AlgSulf0.0). Bare AlgSulf2.0/PCL NPs showed no cytotoxic effect up to 100 $\mu\text{g/mL}$ after 72 hours as shown by trypan blue and up to 100 $\mu\text{g/mL}$ after 48 hours as shown by MTT. The cellular uptake was significantly increased with time up to 24 hours ($p < 0.001$) for Alg/PCL NPs and showed an increasing trend over 24 hours for AlgSulf2.0/PCL NPs ($p = 0.352$). All NPs showed a similar trend in reducing IL-6 in the inflamed media.

Conclusion: Heparin-mimetic IGF-1 loaded AlgSulf NPs represent a novel approach for improving DFUs healing. The developed NPs may also be used for the delivery of other heparin-binding GFs exhibiting broad applications in the therapeutics domain.

Keywords: Nanoparticles, Double emulsion, Diabetes, Diabetic foot ulcers, Alginate Sulfate, Heparin mimetic, Anti-inflammatory

TABLE OF CONTENT

ACKNOWLEDGEMENTS.....	1
ABSTRACT.....	2
ILLUSTRATIONS.....	6
TABLES.....	8
ABBREVIATIONS.....	9
INTRODUCTION.....	13
LITERATURE REVIEW.....	16
2.1. Diabetes and Wound Healing.....	16
2.1.1. Overview of Diabetes.....	16
2.1.2. Diabetic Foot Ulcers.....	19
2.1.3. Wound Healing.....	21
2.2. Extracellular Matrix (ECM) and Wound Healing.....	23
2.2.1. GAGs in Wound Healing.....	23
2.2.2. Growth Factors and Pro-inflammatory Cytokines.....	26
2.3. Current Challenges and Approaches in Drug Delivery.....	28
2.3.1. Delivery of IGF-1 for DFU.....	29
2.3.2. Nanomedicine.....	30
2.3.3. Controlled Drug Release.....	35
2.3.4. Polymeric Nanoparticles Synthesis.....	36
RATIONAL AND HYPOTHESIS.....	45
MATERIALS AND METHODS.....	49
4.1. Materials.....	49
4.2. Methods.....	50

4.2.1. Synthesis of Alg/PCL and AlgSulf/PCL NPs	50
4.2.2. Physical Characterization of the NPs	51
4.2.3. Encapsulation and Release of IGF-1 from Nanoparticles	52
4.2.4. Cytotoxicity of NPs	54
4.2.5. Cellular Uptake of Nanoparticles	57
4.2.6. Enzyme Linked Immunosorbent Assay (ELISA)	58
4.2.7. AlgSulf-coated Alg/PCL NPs as scavengers of inflammatory cytokines	60
4.2.8. AlgSulf-coated Alg/PCL NPs Characterization	61
4.2.9. NPs effect on inflammation	62
4.2.10. Quantitative Real Time Polymerase Chain Reaction (qRT-PCR)	63
4.3. Statistical Analysis	67
RESULTS AND DISCUSSION	68
5.1. Characterization and morphology of AlgSulf/PCL NPs	68
5.2. IGF-1 Encapsulation Efficiency	74
5.3. In vitro Release Rate of IGF-1 from NPs	77
5.4. Cytotoxicity Assessment	79
5.4.1. Trypan Blue Exclusion Assay	79
5.4.2. MTT Assay	81
5.5. Cellular Uptake	82
5.6. AlgSulf-coated Alg/PCL NPs Synthesis and Characterization	86
5.7. AlgSulf-coated Alg/PCL NPs' effect on inflammatory cytokines	88
CONCLUSION	92
APPENDIX	94
REFERENCES	95

ILLUSTRATIONS

Figure

1. Schematic representation of wound healing stages [2].	22
2. Chemical structure of heparan sulfate/heparin disaccharide [1].	25
3. Representation of 3D structure of IGF-1 [1].	27
4. The chemical representation of glycosidic bond conformations of β -D-mannuronic acid and α -L-guluronic [101].	43
Figure 5. Schematic Illustration of the chemical sulfation of sodium alginate. In the first step, sodium alginate is transformed into a tetra-butyl ammonium salt to improve its solubility in the reaction, then the free hydroxyl groups of alginate sulfation take place with $\text{SO}_3/\text{pyridine}$ [101].	44
Figure 6. Schematic illustration of AlgSulf/PCL NPs prepared by double emulsion solvent evaporation technique.	47
Figure 7. Schematic illustration of AlgSulf/PCL NPs formation using the double emulsion solvent evaporation technique.	51
Figure 8. Schematic of the MTT assay.	56
Figure 9. Schematic representation of the Trypan Blue exclusion assay.	57
Figure 10. Serial dilutions of ELISA standard (pg/mL).	59
Figure 11. Schematic illustration of AlgSulf coating on the Alg/PCL NPs.	61
Figure 12. Effect of the degree of sulfation of AlgSulf in the inner aqueous phase of the NPs on their average hydrodynamic size.	69
Figure 13. Effect of the degree of sulfation of AlgSulf in the inner aqueous phase of the NPs and their zeta potential ($p < 0.05$ between the four samples using one-way ANOVA test).	71

Figure 14. Effect of the degree of sulfation of AlgSulf in the inner aqueous phase of the NPs on the PDI of the particles.	73
Figure 15. SEM images of NPs. (a) AlgSulf0.0/PCL NPs (b) AlgSulf0.8/PCL NPs (c) AlgSulf2.0/PCL NPs (d) AlgSulf2.6/PCL NPs.	74
Figure 16. Encapsulation efficiency (EE %) of 1000 ng/mL of IGF-1 entrapped in AlgSulf _{0.0} , AlgSulf _{0.8} , and AlgSulf _{2.0} /PCL NPs.	76
Figure 17. Loading capacity (%) of 1000 ng/ml of IGF-1 entrapped in AlgSulf _{0.0} , AlgSulf _{0.8} , and AlgSulf _{2.0} /PCL NPs.	77
Figure 18. Cumulative release rate (%) of IGF-1 from AlgSulf0.0/PCL and AlgSulf2.0/PCL NPs.	78
Figure 19. % Viability of HaCaT cells using Trypan Blue exclusion assay, n=3.	80
Figure 20. % Activity of HaCaT cells using MTT assay, n=3.	82
Figure 21. Cellular Uptake Efficiency (%) of AlgSulf0.0/PCL NPs and AlgSulf _{2.0} /PCL NPs by HaCaT cells.	84
Figure 22. SEM image of AlgSulf-coated AlgSulf0.0/PCL NPs.	86
Figure 23. FTIR Spectrum of AlgSulf-coated AlgSulf0.0/PCL NPs.	88
Figure 24. mRNA expression of hIL-6 in HaCaT cells after 24 hours of inducing inflammation by LPS and treating the cells with Alg, AlgSulf, IGF-1, AlgSulf0.0/PCL NPs, AlgSulf _{2.0} /PCL NPs, AlgSulf _{2.0} -coated AlgSulf0.0/PCL NPs, and IGF-1 loaded NPs.	89
Figure 25. Amount of hIL-6 released by HaCaT cells into the supernatant after 24 hours of inducing inflammation by LPS and treating the cells with Alg, AlgSulf, IGF-1, Alg/PCL NPs, AlgSulf2.0/PCL NPs, AlgSulf2.0-coated Alg/PCL NPs, and IGF-1 loaded NPs.	90

TABLES

Table

1. Treatment concentrations conversion from $\mu\text{g/mL}$ to $\mu\text{g/cm}^2$.	56
2. Forward and reverse primer sequences used for qRT-PCR. ¡Error! Marcador no definido.	
3. Different steps of qRT-PCR.	64
4. Characteristics of IGF-1 loaded NPs in terms of size, PDI, and zeta potential.	76
5. Size, zeta potential, and PDI of AlgSulf-coated Alg/PCL NPs. ¡Error! Marcador no definido.	

ABBREVIATIONS

A

Alg: Alginate

C

CTGF: Connective tissue growth factor

CVD: Cardiovascular disease

CMC: Critical micellar concentration

D

DM: Diabetes mellitus

DFU: Diabetic foot ulcer

DDS: Drug delivery systems

DMEM: Dulbecco's Modified Eagle Medium

DCM: Dichloromethane

DDW: double distilled water

E

ECM: Extracellular matrix

ELISA: Enzyme-linked immunosorbent assay

EE: Encapsulation efficiency

F

FGF: Fibroblast growth factor

FN: Fibronectin

FBS: Fetal bovine serum

G

GAGs: glycosaminoglycans

GF: Growth factors

GlcA: Glucuronic acid

H

HDL: High-density lipoprotein

HRP: Horseradish peroxidase

HaCaT cells: human immortal keratinocyte cell line

I

IGF-1: Insulin-like growth factor -1

IL-6: Interleukin-6

L

LDL: Low-density lipoprotein

LPS: Lipopolysaccharide

LC: Loading capacity

M

MTT: 3-(4,5-dimethylthiazol-2-yl)-2,5-diphenyltetrazolium bromide

N

NP: Nanoparticles

O

O/W: Oil in water

O/W/O: Oil-in-water-in-oil

P

PDGF: Platelet-derived growth factor

PVA: Poly (vinyl Alcohol)

PCL: Polycaprolactone

PLGA: Poly(lactide-co-glycolide)

PEG: Polyethylene glycol

PM: Polymeric micelles

R

ROS: Reactive oxygen species

qRT-PCR: Quantitative reverse transcription quantitative polymerase chain reaction

S

AlgSulf: Sulfated Alginate

AlgSulf₀: Sulfated Alginate with degree of sulfation 0 (pure alginate)

AlgSulf_{0.8}: Sulfated Alginate with degree of sulfation 0.8

AlgSulf_{2.0}: Sulfated Alginate with degree of sulfation 2.0

AlgSulf_{2.6}: Sulfated Alginate with degree of sulfation 2.6

SEM: Scanning electron microscopy

T

TNF- α : Tumor necrosis factor-alpha

TGF- β : Transforming growth factor beta

V

VEGF: Vascular endothelial growth factor

W

WHO: World Health Organization

W/O: Water in oil

W/O/W: Water-in-oil-in-water

CHAPTER 1

INTRODUCTION

Diabetes mellitus (DM) is a highly prevalent disease and a global public health threat. DM is a chronic metabolic disease characterized by hyperglycemia, and can be classified into three types: type 1, type 2, and gestational diabetes. Patients with DM are susceptible to multiple complications such as diabetic foot ulcers (DFU), a common complication that represents a major health burden and is responsible for 20% of hospitalizations among diabetic patients [1]. DFU is a chronic non-healing condition in DM patients that ultimately leads to infections that might worsen to gangrenes and lead to amputations.

Under normal conditions, the wound healing process occurs as a cellular response to injury. It involves multiple, consecutive, and overlapping steps: hemostasis/coagulation (a), inflammation (b), proliferation (c), and re-epithelialization and remodeling. Various growth factors (GFs) and cytokines are involved in these steps, such as insulin-like growth factor-1 (IGF-1), connective tissue growth factor (CTGF), tumor necrosis factor-alpha (TNF- α), and interleukin-6 (IL-6). The alterations in growth factors levels lead to complications of the wound healing process and result in impaired wound closure [2]. These injuries result in chronic non-healing wounds that become hindered in one or more of the four stages of normal wound healing. In fact, it was shown that DFU patients often suffer from neuropathy, peripheral vascular complications, and abnormal cellular activity that obstruct the diabetic wound healing process [3].

Sulfated glycosaminoglycans (GAGs) are vital in the development of tissues and are key components of the extracellular matrix (ECM), where they play a role in the signaling pathways mainly via interacting and binding to GFs such as IGF-1 and CTGF as well as cytokines [4]. Heparin and heparan sulfate are popular sulfated GAGs that bind to growth factors and activate signaling pathways. By binding to IGF-1, heparin or heparan sulfate induce cellular proliferation, differentiation, and angiogenesis upon intercellular and cell-ECM communications.

Approaches to enhance DFU healing can be achieved by delivering bioactive molecules such as GFs. However, oral drug delivery of IGF is challenged by its fast proteolytic degradation, henceforth reduced bioavailability. Thus, IGF needs to be delivered to the wound site in a novel drug delivery system such as polymeric nanoparticles (NPs) that can ensure its protection and inhibit its premature degradation [5]. The biocompatible polymers currently used in the preparation of nanoparticles are natural, synthetic, or semi-synthetic polymers. Natural polymers include polysaccharides such as alginates (Alg), synthetic polymers include polyvinyl alcohol (PVA) and polycaprolactone (PCL), and semi-synthetic polymers such as chemically sulfated alginates.

Alginates are abundantly used natural biocompatible polysaccharide extracted from brown seaweed FDA approved for drug delivery use [6]. They can be sulfated into sulfated alginates (AlgSulf) and introduced as heparin-mimetics that can bind with high affinity to GF. Besides, PVA and PCL are biocompatible, biodegradable, and non-toxic polymers. PCL has a crystalline structure and as such is characterized by a slow degradation rate which renders it ideal for entrapment and release of drugs over an

extended period of time. Moreover, PVA serves as a stabilizer due to its high fluid absorption capacity and retention rate [7, 8].

To enhance DFU treatment, the development of a drug delivery system that meets favorable requirements is a priority. It needs to primarily provide a moist environment to encourage re-epithelialization of tissues that could be provided by PVA due to its high-water absorption characteristic previously mentioned. It is also important to maintain a sustained and prolonged drug release that could be also ensured upon the inclusion of a PCL shell. Significantly, the use of a mixture of two polymers (PCL and PVA) allows the creation of a balanced hydrophobic and hydrophilic environment that favors cell adhesion and proliferation and stabilizes the cellular degradation state [9].

AlgSulf act as reservoirs for various biological molecules by binding to GFs and cytokines, and providing analogues of cell surface GAGs and mediating GF signaling by creating a biomimetic physical setting for cellular proliferation, ECM deposition, and tissue maturation.

One of the methods to prepare polymeric NPs is double emulsion solvent evaporation technique. The process requires two aqueous phases, an organic phase, and a stabilizer. An energy source is also used for homogenization purposes and it leads to the formation of an outer aqueous layer that encapsulates another aqueous core inside an intermediate oil layer.

CHAPTER 2

LITERATURE REVIEW

2.1. Diabetes and Wound Healing

2.1.1. Overview of Diabetes

DM is a metabolic disorder characterized by high blood glucose levels and by changes in carbohydrate, lipid, and protein metabolism. These changes are caused by alterations in the secretion of insulin, its action, or in both processes [3, 10]. DM is a vastly prevalent disease and is becoming an increasingly important condition globally. In 2010, studies estimated that 285 million adults worldwide had diabetes and this number is expected to rise to 439 million by the year 2030 [11]. Reports in 2017 stated that it costs \$1,200 billion to diagnose, treat, and care for both type 1 and 2 diabetic patients worldwide [3, 12].

Diabetes is a group of metabolic diseases in which the patient suffers from high blood glucose levels, either due to insufficient insulin production, or inappropriate response to insulin by cells in the body. The disease can be classified into type 1, type 2, and gestational diabetes. Type 1 diabetes, or insulin-dependent DM, is characterized by the autoimmune destruction of pancreatic beta cells that leads to deficiency in insulin production. Thus, this type renders its patients completely dependent on an external source of insulin to sustain their lives [13]. The prevalence of type 1 diabetes is usually higher for people under the age of 15 even though only 15-20% of the patients are diagnosed before this age [2]. Moreover, compared to all other ethnic groups, Caucasians tend to present a higher risk of developing type 1 diabetes [14].

Type 2 diabetes, also called non-insulin-dependent DM, is due to a diminished response to insulin which translates to insulin resistance and is associated with dysfunctional beta cells. As the secreted insulin is ineffective in decreasing blood glucose levels, this initially leads to an increase in insulin production to overcome hyperglycemia. However, over time, as the disease progresses, insulin production and secretion decreases causing a permanent state of hyperglycemia in patients [15]. It is estimated that 90% of people with diabetes suffer from this type. Type 2 diabetes patients experience high glucose concentration in their blood in the fasting state or after oral glucose intake. Additionally, they are most often overweight. However, this type of diabetes can be controlled and prevented by following a healthy nutrition regime and establishing a consistent exercising routine. Finally, gestational diabetes is first diagnosed during pregnancy and is defined as carbohydrate intolerance [16]. Gestational diabetes affects approximately 14% of pregnancies and is a risk factor for type 2 diabetes in women [2]. To reduce the morbidity for both the mother and the child, the patient needs to maintain adequate blood glucose levels throughout the gestation period. In the initial stage, women need to treat gestational diabetes through physical exercise and an adequate diet to achieve a normal glycemic level. If these measures fail, insulin treatment should be initiated to achieve better glycemic control [17].

Diabetic complications affect nearly every tissue in the body. The complications associated with hyperglycemia impair the metabolism of carbohydrates, proteins, fats, and electrolytes, all of which disrupt the vascular system. Many endothelial capillary cells are damaged under these conditions, due to the excessive accumulation of glucose. The affected endothelial cells include those lining the capillaries in the nerves, the central and peripheral nervous system, as well as the retina and renal glomerulus. DM

complications are classified into two categories, namely microvascular and macrovascular complications. Microvascular complications include long-term DM-induced complications such as neuropathy, retinopathy, nephropathy, DFU and cardiovascular diseases. Besides, macrovascular complications are mainly coronary and peripheral arterial diseases [4].

Impairment on the endothelial cell level in macrovascular complications is mainly caused by the increase in blood glucose levels, lipids, as well as inflammatory factors. It is also linked to the excessive production of reactive oxygen species (ROS) that in turn leads to vasoconstriction, inflammatory reaction, as well as increase in oxidized low-density lipoprotein (LDL) that increase its' atherogenicity [3].

Atherosclerosis is the increase in lipid deposition, specifically LDL, in the sub-endothelial layer of large blood vessels and is more likely to happen with DM patients. It is promoted by increased permeability and leakage of the endothelial cell layer that are associated with DM-induced endothelial dysfunction [18]. Normally, high-density lipoprotein (HDL) helps in reducing the LDL lipid peroxidation. However, in DM patients, the increased production of ROS induces the oxidation of phospholipids and sterols which leads to reduction in HDL anti-inflammatory and antioxidant activities [18]. Other macrovascular complications include vascular calcification and plaque formation [3].

Current data suggest that rates of all-cause and cardiovascular disease (CVD) mortality are decreasing in individuals with diabetes, trends in other complications of diabetes may become proportionately more prominent in the future [5]. Microvascular diabetic complications are majorly associated with impairment of vascular permeability that affects various body organs including kidneys, nerves, and retina. Prolonged

hyperglycemia can also lead to increased water and protein retention that may further lead to edema [3]. Essentially, the early diagnosis of type 2 diabetes in adolescents and young adults (up to 40 years of age) has been linked to a more aggressive form of the disease, with premature development of serious complications. Together, the above facts highlight the importance of detecting the root causes of diabetes and its complications to best propose strategies for therapeutic interventions for this disorder [19].

2.1.2. Diabetic Foot Ulcers

DFUs are commonly linked to poor glycemic control, peripheral neuropathy, peripheral vascular disease, and immunosuppression. DFU is a frequent complication of diabetes that may lead to severe and persistent infection and, in extreme cases, to lower-extremity amputation. Both DFU and its related amputations pose an economic burden at the level of disability, ensuing hospitalization, and health care that ranges from \$13 to \$15 billion annually. It is estimated that 19-34% of patients with diabetes are likely to develop foot ulcers. The International Diabetes Federation (IDF) reported that 9.1 to 26.1 million people develop DFUs yearly [20]. The United Kingdom demonstrated that the development of DFUs is associated with a 4% mortality within the first 12 months and up to 42% mortality within 5 years. Importantly, patients with DFUs have a 2.5-fold increased risk of death compared to diabetic patients that do not develop DFUs. Therefore, people that develop DFUs mainly suffer from higher mortality, lower quality of life, and higher healthcare expenditure. DFU's treatment costs constitute one-third of the total cost of diabetic care, which was around \$176 U.S. billion dollars in 2012 [21]. The treatment of DFUs is considered challenging since up to 40% of patients relapse within 1 year [17].

The diabetic foot ulceration develops because of a combination of components that together lead to tissue damage. It is an outcome of the interplay between the body's prolonged hyperglycemic state and that of the neuropathic, vascular, and immune system components. Prolonged hyperglycemia subjects nerve cells to oxidative stress that is induced by the formation of cytokines and glycosylation end products. The oxidative stress leads to motor, autonomic, and sensory neuropathy that results in neuropathic foot ulcers [22]. These ulcers are found at typical predisposed locations and they are often circular and surrounded by hyperkeratotic borders that are a result of high-pressure load. Although the ulcer often appears to be a bland and superficial bordered wound, a co-infection of the wound's surrounding tissue commonly takes place. DFUs can be medically classified in a variety of ways, but all of them define the ulcers in terms of the wound depth as well as presence of gangrene or osteomyelitis. According to Wagner's grading of the wound, we note the following: grade 0 refers to the absence of ulcer in the foot with a high-risk factor of complications, grade 1 indicates a partial ulcer, while grade 2 indicates a deep ulcer down to the ligaments and muscles without bone involvement. Moreover, grade 3 refers to a deep ulcer with abscess formation, grade 4 indicates the presence of a localized gangrene, and finally grade 5 indicates gangrene of the whole foot. This classification of DFUs is important since it helps the physicians decide on the appropriate kind of wound dressing for the treatment [22].

2.1.3. Wound Healing

The wound healing process occurs as a natural cellular response to injury. It is a complex process that involves the simultaneous actions of soluble mediators, blood cells, ECM components, and parenchymal cells. The mechanism is constituted of several stages: coagulation or hemostasis (1), inflammation (2), proliferation and re-epithelialization (3), and remodeling (4) as shown in Fig. 1 [23]. Upon injury, hemostasis is established through fibrin plug formation that induces platelets to secrete GF and cytokines (i.e., monocyte chemoattractant protein 1 (MCP-1) and transforming growth factor beta (TGF- β)) which recruit macrophages to the injury site. These factors coordinate biochemical pathways and sequential cell-to-cell and cell-to-ECM interactions. The initial stage involves many types of cells including blood, epithelial, connective tissue, and inflammatory cells along with other soluble factors (1). The coagulation phase is then followed by inflammation mainly driven by neutrophils and macrophages. These inflammatory cells induce the release of critical factors such as IGF-1, CTGF, vascular endothelial growth factor (VEGF), TGF- β , and platelet-derived growth factor (PDGF) (2) [2, 24]. In response to the release of the mentioned critical GFs, keratinocytes and activated fibroblasts start proliferating and migrating from the wound edges into the wound center and produce a collagenous matrix to promote the remodeling of the injured tissue. The damaged ECM is replaced as such by a collagenous matrix along with the formation of new blood vessels, a process named angiogenesis and stops once the wound area is filled with new granulation tissue [10]. Angiogenesis is basically induced by the angiogenic factors including VEGF and fibroblast growth factor (FGF) that in turn promote the proliferation of fibroblasts and endothelial cells (3). Finally, wound closure is implemented by contraction of the

wound edges due to matrix deposition and myofibroblasts differentiation (4). These phases may overlap or occur consecutively as they are not associated with well-defined time frame [10, 24].

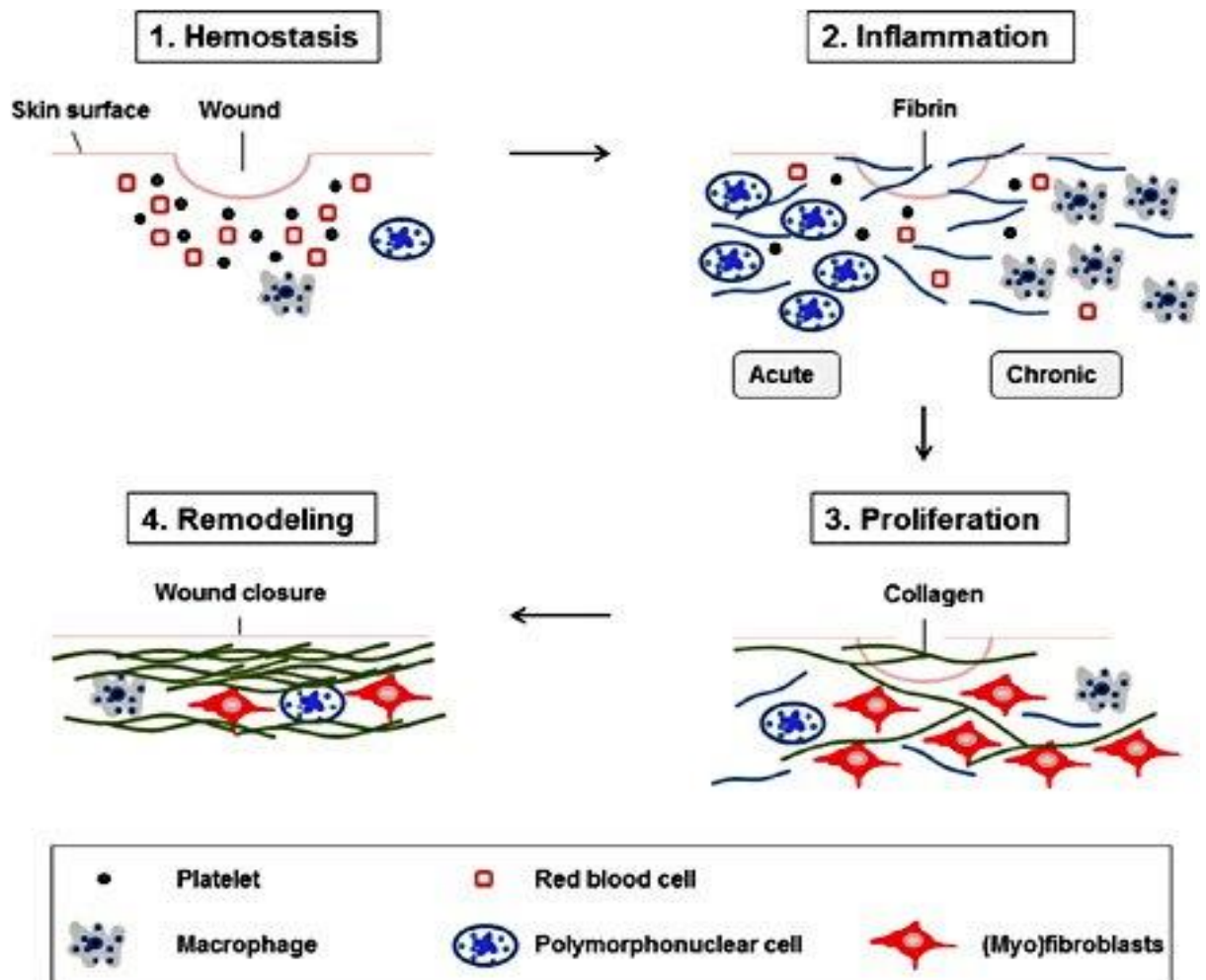


Figure 1. Schematic representation of wound healing stages [2].

In diabetic patients, the normal wound healing process is attenuated due to neuropathy that causes permanent damage in nerve tissues. The increase in glucose level as well as the decrease in blood flow result in loss in the peripheral nerve fibers, thus, ulceration might occur. Diabetic neuropathy occurs in both type 1 and type 2

diabetes, mainly in older patients. Approximately, 50% of diabetic patients develop nerve damage in some extremities after 10-20 years of diagnosis with diabetes [25]. The chronic wounds and prolonged inflammation are more prevalent in diabetic patients due to disruptions in the events of hemostasis, inflammation, proliferation, and remodeling. Dysregulated release takes place at the level of certain matricellular proteins such as CTGF, GFs such as IGF-1, and cytokines like TNF- α and IL-6. DFUs that are not effectively treated may ultimately lead to partial or complete lower limb amputation, a tremendous burden on the patients and the economic healthcare system worldwide [26, 27].

2.2. Extracellular Matrix (ECM) and Wound Healing

2.2.1 *GAGs in Wound Healing*

The wound healing process is an interaction between different cell types and the ECM. ECM synthesis and deposition are crucial for the implementation of the dynamic healing process as it provides a cascade of molecules that play an integral role in wound healing. These molecules include structural proteins such as collagens, multidomain adhesive glycoproteins such as fibronectin (FN), GAGs, and matricellular proteins. GAGs are key structural and functional ECM polysaccharides that activate both inter and intracellular signaling pathways. They play an essential role in wound repair activity through all the phases of repair by providing both a scaffold support as well as a signaling role [28]. Also, GAGs control the sequestration and release of GFs through which they turn into tetrameric complexes and their receptors get stabilized. The molecular mechanisms that command the activity of GAGs in biological events are still being elucidated and several studies have identified a correlation between GAGs

sulfation and binding of growth factors and as such their downstream cellular responses [29-31].

Binding of GFs to sulfated GAGs, protects them from degradation and denaturation, prolongs their plasma stability, and enhances their biological activity. Indeed, the levels of heparin, a widely known GAG, were found to be elevated in wounds as they can provide both scaffold support and storage for the necessary molecules. These molecules include heparin-binding GF's, proteolytic enzymes, and protease inhibitors. Heparin also contributes to the recruitment of inflammatory cells. Besides, heparin binds to matrix proteins such as FN and laminin, which provide a more stable scaffold for the present cells [32, 33].

GAGs are carbohydrates composed of repeated linear disaccharide units of uronic acid and glucosamine sugar residues that are crucial in tissue development. They are negatively charged due to the presence of sulfate groups except for hyaluronan that has an overall negative charge because of glucuronic acid (GlcA) residues. Some GAGs are further sulfated in the Golgi apparatus and exhibit as such heterogeneous sulfation patterns and degrees of sulfation (DS, which represents the average number of sulfate groups per disaccharide repeating unit ranging from 0 for non-sulfated to 4 for fully sulfated polysaccharides). Sulfated GAGs act as reservoirs for various biological molecules by binding to and sequestering GFs, proteins, chemokines, and cytokines via electrostatic interactions regulated by their DS [33].

Heparins and heparan sulfates are GAGs that have the most complex structure among other GAGs, represented in Fig. 2. They are made of repeating disaccharide units of GlcA and N-acetylglucosamine (GlcNAc) present in the form of repeating

GlcA β 1,4-GlcNAc α 1,4 units [34]. Heparins play a key role in chemical signaling between cells. The prevalence of sulfate and carboxylate groups endow heparin with a high negative charge which mediate its electrostatic interactions with many proteins, such as heparin-binding GFs, proteases, and chemokines [35].

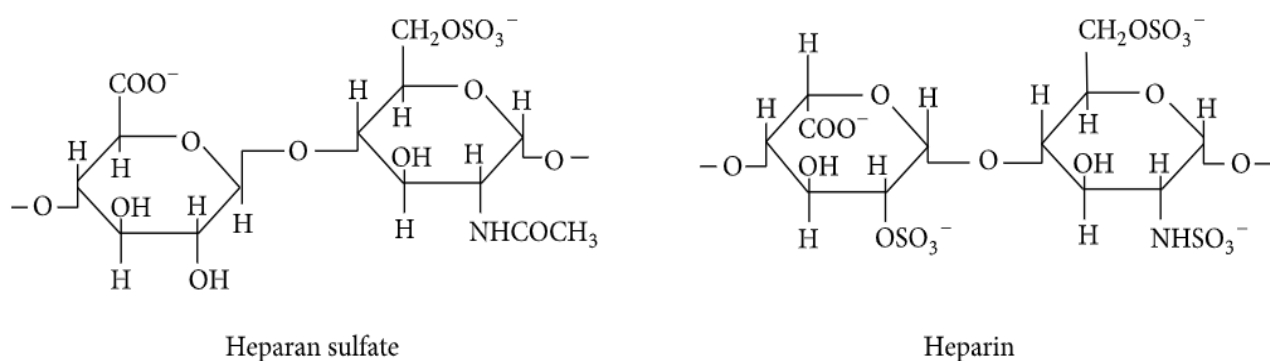


Figure 2. Chemical structure of heparan sulfate/heparin disaccharide [1].

Heparin-binding proteins include, but are not limited to, FGF, IGF, CTGF, PDGF, and FN. These GFs and cytokines are involved in the consecutive and overlapping steps of wound healing, as discussed earlier. However, many of these factors were found to be deficient in chronic wounds specifically diabetic ones. Accordingly, migration and proliferation of keratinocytes and fibroblasts become dysregulated leading to non-healing wounds [32].

Heparin, the most acidic and sulfated form of GAGs is clinically presented as an anticoagulant and anti-inflammatory agent. Heparin and heparan sulfates affect several signaling pathways in cells by regulating the activity of heparin-binding GFs as well as proteolytic enzymes. While heparin may have safe anti-inflammatory actions, its anti-

coagulant function might exhibit undesired hemorrhagic complications. Thus, it is often administered in an encapsulated form in nanoparticles or covalently conjugated to hydrogels to provide a sustained and safe release of the anti-coagulant [36, 37].

2.2.2. Growth Factors and Pro-inflammatory Cytokines

IGF-1

IGF-1, among other GFs, can influence the healing process of wounds and ulcers through the stimulation of chemotactic activity in endothelial cells, keratinocyte and fibroblast proliferation, and re-epithelialization [38, 39]. Thus, it modulates tissue growth and repair. IGF-1 is an anabolic single-chain polypeptide made up of 70 amino acids and represented in Fig. 3 [40]. It has an amino acid sequence close to that of insulin with similar biological effects such as promoting cell cycle progression and cellular growth. It is a heparin-binding GF that can also bind with high affinity to sulfated alginates (AlgSulf). Overall, it is a potent GF in the body that affects the stimulation of DNA synthesis, cellular proliferation, and glucose transport [39, 41, 42].

Importantly, *in vivo* studies showed that IGF-1 induces keratinocyte proliferation and its levels significantly increase in the wound fluid and plasma during the process of skin cells healing. In diabetic patients however, the levels of IGF-1 in wound fluid and plasma were found to be diminished which disrupts the wound healing process. This supports the idea of the implication of IGF-1 in wound healing [43, 44].

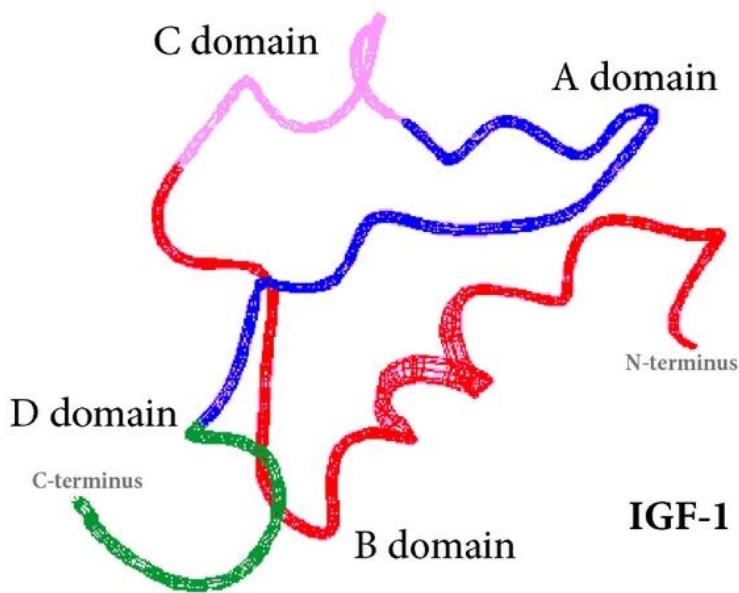


Figure 3. Representation of 3D structure of IGF-1 [1].

CTGF

CTGF is an ECM-associated heparin-binding protein that binds directly to integrins. It is synthesized by fibroblasts and stimulates the proliferation and chemotaxis of these cells. In the case of wounds, CTGF expression increases as it is involved in granulation tissue formation, ECM deposition and remodeling, and re-epithelialization. More studies show the key role of CTGF in promoting endothelial cells proliferation, migration, adhesion, and angiogenesis [43, 45].

Interleukin-6

IL-6 is a pro-inflammatory heparin-binding cytokine that can also have an anti-inflammatory activity. It is produced and secreted by neutrophils and monocytes and is crucial for the initiation of the healing process. IL-6 levels increase quickly after wounding and persist in case of old chronic wounds. IL-6 exhibits mitogenic and

proliferative effects on keratinocytes. It also attracts neutrophils via chemical signals [44]. Significantly, studies showed that IL-6 binds to heparin mimetic AlgSulf that can help reduce inflammation in diabetic patients [46, 47]

TNF-

TNF- α is a proinflammatory heparin-binding cytokine that participates in the endogenous cytokine response to wound healing and repair. It is a pleiotropic cytokine primarily secreted by macrophages. It promotes wound healing due to its ability to stimulate angiogenesis as well as induce proliferation of fibroblasts [48]. It is also suggested that TNF- α stimulates inflammation and inhibits endothelial cells growth.

2.3. Current Challenges and Approaches in Drug Delivery

Introducing new drugs into the pharmaceutical market is a strenuous and expensive process. Several experimental and clinical trials take place in which approximately one out of thousands of compounds become validated and introduced into the market. Many drug compositions suffer from poor pharmacodynamic and pharmacokinetic properties. These properties are mainly affected by the route of administration, dosage, drug distribution, excretion, and elimination. Other concerns in drug generation are low half-life, poor availability, cellular toxicity, and adverse effects of the drug components or metabolites. Delivering the drug towards specific tissues or cells while achieving minimum toxicity and maximum therapeutic activity can be controlled by choosing the most convenient drug administration route. It is both important and challenging to maintain the delivered concentration of the drug within its therapeutic window [49].

The oral route is considered the most favorable administration route due to its convenience and improved patient compliance, especially in chronic conditions. However, the oral route faces many limitations including the exposure to a wide range of pH environments, enzymatic degradation, and poor permeability across the epithelium tissue of different organs [50]. Orally administered drugs are also characterized by their low bioavailability. They are rapidly eliminated from the body either intact or after being bio-transformed by enzymes or acid-catalysis before reaching the systemic circulation or due to insufficient intestinal absorption [50]. To increase their bioavailability, drugs can be administered via direct injection into the bloodstream. However, drugs with a short half-life, such as GFs, still face the risk of being cleared quickly from the body. A traditional way to overcome this limitation is by increasing the concentration of the GF in the dosage form, risking a potential undesired toxic effect and an unwanted increase in the drug's price. Accordingly, recent advanced drug delivery approaches tend to deliver GFs using novel drug delivery systems (DDS) that can protect and enhance the drugs' half-life without increasing its dose.

2.3.1. Delivery of IGF-1 for DFU

Local delivery of IGF-1 has been a long-lasting challenge for researchers and physicians. The pharmacokinetic and pharmacodynamic properties of therapeutic IGF-1 are influenced by the administration route and the dosage form. A successful and desired therapeutic outcome requires overcoming obstacles like poor bioavailability and the potential side effects. Oral administration of IGF-1 is limited by the rapid proteolytic degradation of the GF, thus leading to poor bioavailability [51].

Considerable research efforts have been devoted to the development of alternative modes for safe and effective delivery of GFs. Significantly, delivering GFs using a DDS ensures enhanced pharmacokinetics and increased clinical efficacy of the drugs.

2.3.2. Nanomedicine

Nanomedicine is a broad interdisciplinary field that bridges nanoscience, nanoengineering, and nanotechnology interacting with the life sciences. It is distinct from typical medical fields as it consists of applying materials and technologies at the favorable nanoscale. Like medicine, the aim of nanomedicine is to continuously enhance the clinical medical applications while fulfilling all the needed safety and ethical criteria [45]. Nanomedicine refers to the application of nanotechnology-based therapeutics and materials in monitoring, identifying, preventing, and treating injuries, diseases, and damaged tissues in biological systems [48]. It is expected that nanomedicine will lead to the development of improved drug formulations, medical devices, and biosensors for early diagnosis and treatment of a wide range of diseases with high specificity, efficacy, and personalization, with the objective being to enhance patients' quality of life. The application of nanomedicine includes the development of nanosystems utilized in disease treatment, diagnosis, and monitoring. Nanosystems can be designed to have different compositions and physiochemical structures to meet desired properties depending on their ultimate application. Examples on these nanosystems are liposomes, micelles, and nanoparticles, discussed further below. Nanomedicine has raised exciting expectations for many medical problems, especially chronic ones [52, 53].

Liposomes

Liposomes are small vesicles with a spherical shape that have an internal aqueous environment bounded by one or more phospholipid bilayer membranes. They can be produced from cholesterol, glycolipids, sphingolipids, non-toxic surfactants, and long chain fatty acids.

Liposomes are DDS that can be loaded with a variety of molecules such as small drug molecules and proteins. They are already present at the pharmaceutical market as DDS for the encapsulation of chemotherapeutic drugs such as Doxorubicin and anti-fungal agents such as Amphotericin B. The advantage of liposome-based DDS is that they can be formulated with different sizes, compositions, charge, and rigidity. Thus, they can be modified to achieve the desired controlled drug delivery. Their size ranges between several micrometers down to 30 nm and can serve as reservoirs for hydrophilic and hydrophobic drugs, due to their unique structure. In fact, hydrophilic drugs can be encapsulated in their inner aqueous compartment while hydrophobic compounds can be entrapped between the phospholipid bilayers, making liposomes ideal DDS for co-delivery of drugs.

Many factors contribute to classifying liposomes as successful DDS. They solubilize and deliver lipophilic drugs that are difficult to administer intravenously. In addition, the encapsulated drugs are protected from metabolizing enzymes; conversely, body components such as the tissue injection site are protected from high full doses of the drugs [54-56]. Advantageously, liposomes can cross the blood-brain barrier because of their lipophilic nature. Thus, they can also be used to encapsulate and deliver hydrophilic drugs that are not able to normally cross the blood-brain barrier. They are

also non-toxic, biocompatible, completely biodegradable, and non-immunogenic. However, the drawbacks of using liposomes as DDS are their short-half life, leakage and fusion of the encapsulated drugs, and low solubility in biological fluids [57].

Micelles

Micelles are spherical particles that consist of an inner hydrophobic core and outer hydrophilic shell that can form spontaneously when placed in an aqueous medium. This allows micelles to stay in the blood or targeted tissue for a long time without being recognized and shed by enzymes and phagocytic cells. This longevity is an important advantage for micelles to be considered as favored DDS. It also helps provide gradual accumulation of the drug in the targeted tissue. Being in the micellar form, they can entrap drugs with poor solubility thus, increase their bioavailability. The encapsulated drug is as such well protected from possible inactivation by biological enzymes, which increases its plasma stability and decreases its undesirable side effects [58].

Polymeric micelles (PM) are considered among the most promising DDS especially for drug targeting applications in cancer. They are formed via self-assembly of block copolymers placed in an aqueous medium and made up of two main components: the inner core and outer shell [59]. The outer shell of PM controls the pharmacokinetic behavior of the drugs in vivo, while the inner core is responsible for the loading capacity, stability, and release rate of the drug. Compared to other DDS, such as liposomes and nanoparticles, PMs possess higher drug loading capacity and improved stability. Their high drug loading capacity is due to the large volume of their drug-loading hydrophobic inner core. Despite these advantages, the release of the drug

from PM remains dependent on the critical micellar concentration (CMC) above which aggregates of large sizes of these micelles are formed [60, 61]. Below this CMC, micelles disassemble into free surfactants and lose their structure. As a result, the drug of interest entrapped in the hydrophobic region of a micelle core becomes insoluble due to the loss of the drug carrier micellar structure. This alters the therapeutic performance of the drug carrier and reduces its bioavailability [62].

Nanoparticles

In the therapeutic field, micromaterials are widely implemented in treatment of millions of patients annually. However, they cannot cross the blood vessels, nor enter the cells after being injected due to their relatively large size. Therefore, NPs with a size ranging between 10 and 1000 nm have been employed to overcome this limitation and have become significant biological delivery vehicles. NPs are nanosized structures that provide a revolutionary potential for a range of medical applications such as diagnostic imaging, drug delivery, implantable devices, and others. They can be developed to have a wide variety of sizes, shapes, and compositions which enables their usage in various fields such as drug delivery where they can serve as pharmaceutical carriers [63]. NPs can be employed in a wide range of applications such as therapy, diagnosis, and imaging. In addition, the small size range of NPs gives them the advantage of having a large surface area to volume ratio, thus ensuring a high adsorption capacity [64]. The surface area of NPs represents the summation of the areas of the exposed surface of NPs per its mass, consequently, the size of NPs is inversely proportional to their surface area [65]. Delivering drugs, such as GFs via biomaterials, liposomes, NPs, and PM, exert greater therapeutic effects on healing than freely delivering them. The

delivery systems are best designed to ensure that the drug reaches the desired targets in a spatially and temporally controlled manner [66]. The conventional oral and parenteral routes of drug administration have several disadvantages such as altered pharmacokinetic properties and widespread distribution of the drug. Moreover, genetic polymorphisms, overexpression of efflux pumps, and the development of drug resistance may attribute to decreased drug efficacy. All of these can be overcome with nanostructure-mediated drug delivery to administer the drug at the desired site of action. NPs offer an opportunity to achieve specific accumulation of drugs in the required site with less toxicity. The NPs used in drug delivery include quantum dots, nano-shells, lipid, polymeric, micellar, and gold NPs.

Biocompatible polymeric NPs

For polymers to be safely used in temporary biomedical systems, such as in drug delivery, tissue engineering, and wound dressings, they are crucially required to be biodegradable. Biodegradable polymeric NPs are favored for use as DDS because of their subcellular size, their ability to provide controlled release properties, and their biocompatibility with cells and tissues [67]. Mainly, polymers with biodegradable characteristics consist of carbohydrate, ester, or amide backbones that have enzymatically labile bonds able to break down into smaller monomer units. In addition, these byproducts are ought to be biocompatible as well as produce desirable effects without causing inflammation or immune reactions in the host. These advantages make biocompatible and biodegradable polymer-based NPs of great interest [67, 68].

Polymeric materials used to prepare polymeric NPs are commonly categorized into natural and synthetic polymers. Natural polymers readily exist in nature and can be

derived from a wide range of inexpensive plant- or animal-based sources. On the other hand, synthetic polymers are derived from pre-existing raw material. The natural polymeric materials include natural polysaccharides such as hyaluronic acid, chitosan, cellulose, and alginate (Alg); and natural proteins, such as albumin, elastin, and collagen. Synthetic polymers include, but are not limited to, polylactic acid (PLA), poly(vinyl alcohol) (PVA), poly(lactide-co-glycolide) (PLGA), and poly(caprolactone) (PCL) [69-71]. Polymer-based NPs have gained increased interest in the research field of drug delivery due to their controlled drug release property [72].

To further improve polymeric-based DDS, a mixture of both synthetic and natural polymeric materials can be used to obtain NPs with favorable properties. In addition, polymeric NPs can be developed from various types of polymers with different physical and chemical properties. For instance, they can be of natural or synthetic nature, biodegradable, or non-biodegradable, hydrophilic or hydrophobic NPs based on the polymeric materials used.

2.3.3. Controlled Drug Release

It is crucial and important to maintain the amount of the drug delivered within its effective therapeutic index while controlling the drug release rate, especially when delivering GFs. Controlled release formulations can permit to reduce the amount of drug necessary to cause the same therapeutic effect in patients or even prolong drug dosage interval which can increase patient compliance. When the drug is administered freely, its concentration in the blood increases immediately until it reaches its peak and then drops down within hours. To overcome this, controlled drug delivery is utilized by either adjusting the release rate of the drug over time or transporting the drug to the

target tissue. DDS can enhance the therapeutic effect of GFs while decreasing the administered dose, maintain the drug's safety profile, and optimize its targeted delivery [73].

The release rate can be decreased to ensure slow release over time such that the concentration of the drugs will be maintained within its therapeutic range for a longer time. This can be implemented by conjugating the drug to natural or synthetic carriers to stabilize it. In many controlled release-based DDS, and upon the placement of the drug in the release medium, an immediate release of a large amount of the drug takes place. This phenomenon is called the burst release effect and it occurs by means of drug diffusion, desorption, or erosion. It takes place before the drug reaches a stable release profile. The released drug concentration during the initial burst release phase varies between high and low depending on both the drug and carrier. For instance, high porosity level in the carrier is likely to lead to high burst release while robust crosslinking of the drug with the carrier's surface would ultimately limit the initial desorption of the drug [73, 74]. In the case of wound healing, DDS with controlled release is favored because they can help limit drug degradation by the wound proteases, avoid frequent administration of the drug, as well as enhance and prolong the treatment's efficacy [74].

2.3.4. Polymeric Nanoparticles Synthesis

NPs can be formed through different synthesis approaches. They are basically divided into two main methods, namely: bottom-up and top-down methods. The bottom-up approach is a nanofabrication-based method that starts at the molecular level, and through a growth process, forms the final nanostructure assembly. The

disadvantage of this method is the batch-to-batch variety and broad NP size distributions. Inversely, the top-down method is based on processing large materials down to generate NPs. The first method requires emulsion polymerization or polycondensation, whereas the second one can be achieved via emulsion solvent evaporation or solvent diffusion, electrodynamic co-jetting, or soft lithography. Solvent emulsion technique is favored over other methods of fabrication due to its simplicity and ease of tuning. NPs formation can be implemented via three processes, which are single emulsion solvent evaporation, double emulsion solvent evaporation, or by emulsion solvent displacement. Emulsions are generally preferred as they do not require polymerization reactions and, thus, lack the presence of any impurities including monomers, unreacted agents, or catalysts. Furthermore, NPs size control may be achieved by tuning process parameters such as speed and amplitude of emulsification, type and concentration of surfactants and polymers, and the temperature and pressure during solvent removal [75, 76].

Emulsion-solvent evaporation technique

The principle of emulsion is the mixture of two or more immiscible liquids, in which one or more phases are dispersed in another one. Emulsions could be water-in-oil (W/O), oil-in-water (O/W), oil-in-water-in-oil (O/W/O), or water-in-oil-in-water (W/O/W). The emulsion process is usually thermodynamically unstable, thus emerges the need for surfactants and stabilizers to stabilize emulsion droplets. This technique is widely used in the preparation of polymeric NPs, using different natural and synthetic types of polymers depending on their solubility [77].

The emulsion-solvent evaporation process is the most frequently used technique for preparation of NPs because it is relatively simple to perform and it provides NPs prepared from purified polymers. This technique delivers consistent results with respect to size distribution. It is applied for engineering polymeric nano- and microparticles which can entrap various types of drugs such as proteins and peptides [78]. The product of this technique depends on many factors, including type of emulsion, type of organic solvents and stabilizers, process conditions, type and concentration of the polymers used, and amount and type of drug to be encapsulated.

Single emulsion-solvent evaporation technique

This technique consists of emulsification of a dispersed phase that contains polymers, solvents, and/or drugs in another continuous phase. The two phases mixed form large emulsions, and then can be broken down into smaller emulsions, at the micro- or nanoscale, by applying high pressure using a mechanical homogenizer or acoustic waves from a sonicator. Classically, this is followed by the evaporation of the organic solvents from the oil phase under stirring conditions to reach a point of insolubility and promote the solidification of the hydrophobic polymer, and yield as such solid NPs. The NPs are then washed, collected by ultracentrifugation, and freeze-dried in their final form.

Double emulsion solvent evaporation technique

Herein, to form W/O/W double emulsion, a hydrophobic polymeric solution (organic phase, O) is dissolved in an inner aqueous phase (W1) until homogenization forming the primary emulsion (W1/O). While applying acoustic waves or high pressure, an external aqueous phase is added to the primary emulsion forming small nanoscale

secondary emulsions (W1/O/W2), This is followed by the evaporation of the water-insoluble organic solvent (i.e., dichloromethane or chloroform) with subsequent polymer precipitation encapsulating the drug or active material [7, 8]. The double emulsion solvent evaporation technique is considered one of the most useful, fast, and cost-effective techniques to engineer polymeric NPs that can encapsulate different drug types (hydrophobic and hydrophilic). Among frequently used synthetic polymers in the formation of W1/O/W2 emulsions are PCL, polyethylene glycol (PEG), PLGA, and PVA.

Poly (Vinyl Alcohol)

PVA is a synthetic polymer that has been used for the past 30 years in several medical and nonmedical devices. It is a biologically compatible material that is stable in animals and humans with suitable biomechanical properties that make it a promising polymer to be used in medical and biomedical research. PVA is approved by the FDA, thus it is used in different medical applications as well as in food products [79].

PVA is a linear polymer produced via partial or full hydrolysis of polyvinyl acetate to remove the acetate groups. It is biocompatible, non-toxic, non-carcinogenic, bio adhesive, and highly stable. Its high stability against organic solvents favors its use as a surfactant in double emulsion solvent evaporation techniques [79, 80]. PVA does not undergo chemical or enzymatic degradation, rather it breaks down and its dissolution into the medium is driven by erosion. PVA is hydrophilic and has high water retention capacity and can therefore offer moist conditions for the ulcer which makes it favorable for wound healing applications. In addition, because of its stability at

high temperatures and pH values, it is advantageously used to stabilize NPs. Thus, it helps NPs stay stable facing the harsh force in freeze-drying [8].

Polycaprolactone

PCL is a synthetic polymer synthesized by ring-opening polymerization of caprolactone using a catalyst (i.e., SnO_2) and heat. Through co-polymerization, the physiochemical properties of PCL can be modified which in turn helps change its solubility and degradation pattern characteristics [7]. It is a biodegradable polymer that is eliminated from the body via an innate metabolic process. After degradation, it releases carboxylic groups that increase the pH of the environment which becomes basic in chronic wounds. Due to its biodegradable, biocompatible, bioabsorbable, and non-toxic characteristics, it is used in medical implants, dental splints, and DDS like NPs.

PCL is a hydrophobic polymer and is characterized by a crystalline structure which provides it with a slow degradation rate compared to other polymers such as PLGA. Accordingly, it allows the encapsulation and sustained release of drugs over an extended period of time [7]. Moreover, owing to its crystalline structure and its low melting point (59-60°C), PCL promotes good drug permeability in addition to a slow drug release rate. In fact, the degradation of PCL is considerably slow compared to PLGA because the close packed macromolecular arrays delay fluid access in its bulk. Therefore, PCL can be used for prolonged and sustained drug release purposes [81, 82]. Importantly, like PVA, PCL is an FDA-approved polymer and already used in biomedical applications, such as NPs and scaffolds. Significantly, mixing PCL and

PVA would allow the creation of a balanced hydrophobic/hydrophilic environment that favors cell adhesion and proliferation [9].

Poly (lactic-co-glycolic acid)

PLGA is one of the most used biodegradable polymers in the development of nanomedicine. Similarly, to PCL, PLGA is a biocompatible and FDA approved polymer for medical applications. It is produced via ring opening polymerization of two different monomers of glycolic and lactic acid that are then linked together by ester binding. Its hydrolysis in the body leads back to these two metabolite monomers. Furthermore, these monomers are easily metabolized by the body via Krebs's cycle; thus, PLGA is associated with minimal systemic toxicity. PLGA is already being used in the synthesis of NPs, hydrogels, and scaffolds. Compared to PCL, PLGA has a faster biodegradation rate due to its amorphous structure, hence, leading to a more rapid release of the encapsulated drug. The release kinetics of encapsulated drugs from PLGA microparticles and NPs depend on several factors such as PLGA molecular weight, lactide/glycolide ratio, and PLGA end-groups. The end-group of PLGA is a factor that affects the polymer's hydrophilicity degree. In general, studies showed that PLGA copolymers carrying free carboxylic end groups cause higher initial burst release rates compared to the end-capped polymer [83, 84].

Alginate

Alginate (Alg) is a natural anionic polysaccharide typically extracted from brown seaweed. It includes linear copolymers with blocks of (1,4)-linked- β -D-mannuronic acid (M) and α -L-guluronic acid (G) residues, shown in Fig. 4. The M/G

ratio present, as well as the sequence of these residues in the polymer affect the absorbance, softness, viscoelasticity, and swelling properties of the alginate. The gelation of alginate takes place by combining the aqueous alginate solution with ionic cross-linking agents, such as divalent cations (i.e., calcium and magnesium ions). These cations bind to the G blocks that then form junctions with other G blocks of the adjacent polymer chains generating what is termed as the “egg-box” model of cross-linking. The gelation property makes alginate a preferred candidate for GFs and proteins delivery since they can be protected from degradation until they are released. Another crucial property of Alg is its biodegradability. The degradation process of Alg consists of a proton-catalyzed hydrolysis that is a time-, temperature-, and pH-dependent process. As they are polysaccharides, Alg are subject to hydrolysis or degradation in strong acids, especially at elevated temperatures [85, 86].

Alg polymers are FDA-approved and currently being used in various biomedical applications. Alg is a successful candidate for the delivery of low molecular weight drugs, especially when a primary or secondary bond between the drug and the Alg polymer can be formed since it regulates the drug release kinetics. Importantly, heparin-binding GFs (i.e., IGF-1 and CTGF) can bind reversibly and with high affinity to Alg which enables slow and controlled release of the GFs encapsulated within Alg NPs. Alg is also extensively used in the treatment of acute and chronic wounds offering Alg-based dressings with advantageous features. Significantly, Alg-based wound dressings provide moist wound environment which facilitates the healing process. In its dry form, alginate dressings absorb the wound fluid which then allows it to form a gel, supply water to a dry wound, and prevent bacterial infection at the wound site. It can also

promote tissue granulation, rapid epithelialization, and overall healing of the wound [85, 87, 88].

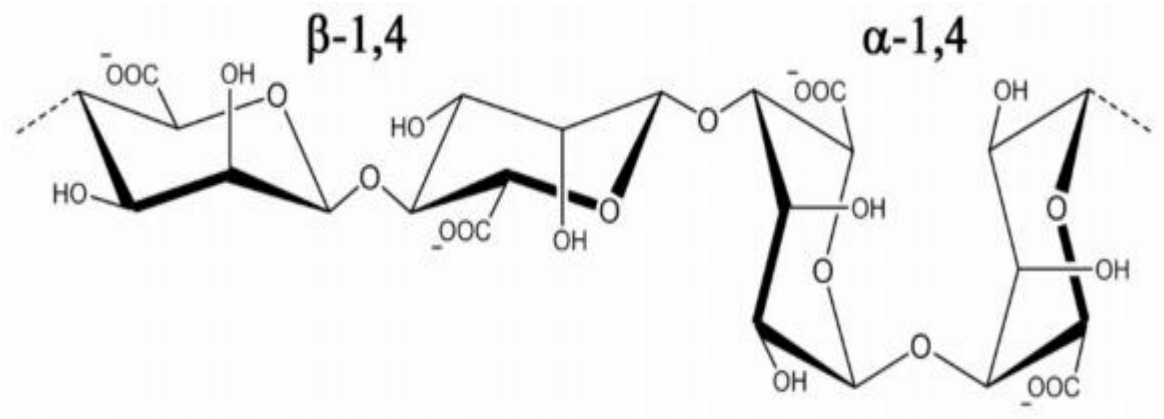


Figure 4. Chemical structure of a disaccharide unit of alginate, showing the β -1,4 and α -1,4 linkages between the pyranose and furanose rings, respectively. The structure includes carboxylate groups ($-\text{COO}^-$) and hydroxyl groups ($-\text{OH}$).

Alginate Sulfate

The use of heparin and sulfated GAGs in long-term biomedical applications is limited due to their rapid turnover *in vivo* and difficulty in purifying sulfated GAGs of homogeneous structures. Thus, it was important to find other stable analogues for their use in tissue engineering and drug delivery fields. AlgSulf were presented by Cohen *et al.* as promising polymers that can bind to multiple heparin-binding GFs (i.e., IGF-1, CTGF, VEGF), highlighting AlgSulf's potential in serving as GFs' reservoir and slow prolonged release system in drug delivery [44].

Pure Alg sulfation can take place using different sulfating agents such as sulfuric acid-carbodiimide, chlorosulfonic acid formamide, or various $\text{SO}_3/\text{complexes}$ [89]. $\text{SO}_3/\text{pyridine}$ was present as a mild sulfation agent that allows the control over the DS of AlgSulf. As present in Fig. 5, the esterification of the hydroxyl groups of sodium

alginate takes place. Due to their polysaccharide nature and presence of sulfate groups on their backbone, AlgSulf exhibit mucoadhesive properties and mimics heparin and sulfated GAGs such as chondroitin sulfate and heparan sulfate. These AlgSulf properties induce the activation of signaling pathways by creating a biomimetic physical setting for cellular proliferation, ECM deposition, and tissue maturation [90]. Like heparin and heparan sulfate, AlgSulf also possesses anticoagulant properties [6]. Interestingly, studies showed a dual role of AlgSulf in signaling through suppressing and promoting cellular signaling pathway by binding to soluble factors such as inflammatory cytokines and GF. This is attributed to the non-specific binding of AlgSulf to proteins. Like sulfated GAGs, AlgSulf have a low specificity binding property, by which they can bind and sequester inflammatory cytokines such as IL-6, IL-1b, and TNF- α and suppress as such inflammatory events [46, 90].

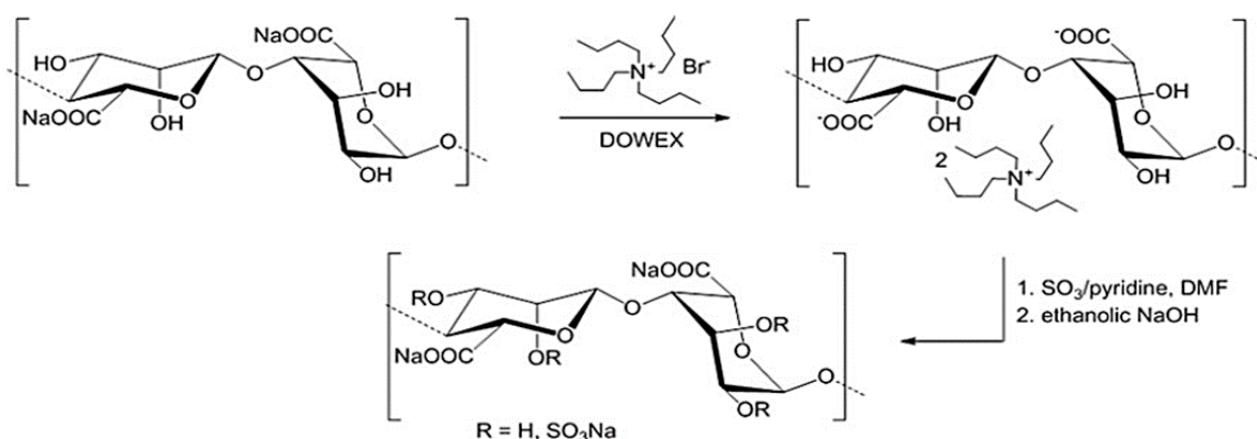


Figure 5. Schematic Illustration of the chemical sulfation of sodium alginate. In the first step, sodium alginate is transformed into a tetra-butyl ammonium salt to improve its solubility in the reaction, then the free hydroxyl groups of alginate sulfation take place with $\text{SO}_3/\text{pyridine}$

CHAPTER 3

RATIONAL AND HYPOTHESIS

Diabetic foot ulceration remains an illustration of a chronic wound condition developed by diabetic patients. It is associated with a decreased production of the endogenous stimulants responsible for the healing process, such as heparin-binding GFs, cytokines, and other ECM molecules, resulting in a slow-paced or even failed wound repair. Heparin-binding GFs, including IGF-1, are among the potent stimulants that have a low half-life and a low stable nature as they are easily affected by the harsh microenvironmental changes in *in vivo* settings. Thus, it is crucial to ensure a longer half-life, increased stability, and decreased degradation rate of these GFs through controlled drug delivery systems as a mechanism to enhance the DFU healing process. An ideal approach is through using biodegradable polymers to form NPs that are stable and can permeate biological barriers compared to larger particles [91]. Accordingly, the encapsulated GF is protected from early degradation while maintaining its dosage within the desired therapeutic index with a controlled drug release rate. This can be achieved by engineering NPs using the double emulsion solvent evaporation technique where the water-soluble GFs are encapsulated in biodegradable polymers that increase the GFs stability. Herein, the NPs were prepared using a heparin-mimetic AlgSulf core in which IGF-1 is embedded and protected by a hydrophobic PCL outer shell. Moreover, as heparin-mimetic AlgSulf is known to have high affinity to heparin-binding GFs, including IGF-1, it is anticipated to help promote a prolonged and slow-release rate of the entrapped drug from the NPs. In addition to the high affinity to heparin-binding GFs, AlgSulf is proposed to exert anti-inflammatory properties by

binding and sequestering inflammatory mediators such as IL-6 [46]. Additional advantage of using these NPs as DDS is related to their small size, which implicates that they could be taken up by cells via endocytosis [92]. Therefore, the proposed NPs are expected to represent a promising therapeutic modality to promote more effective and faster healing of DFUs.

Aim 1: Synthesis and characterization of IGF-1 loaded AlgSulf/PCL nanoparticles by double emulsion solvent evaporation technique.

Hypothesis: Typically, as the DS of alginate rises, the number of sulfate moieties binding to free hydroxyl groups increases. In the presence of cationic cross-linking agents, such as Ca^{2+} , the electrostatic interactions occurring between positively charged Ca^{2+} and negatively charged groups within alginate sulfate become weaker as less cross-linking occurs, hence, softer, and smaller NPs are formed. Therefore, we expect the size of the NPs to decrease as the DS of AlgSulf in the inner aqueous phase increases, rendering them more favorable for *in vitro* and *in vivo* use.

Also, IGF-1 is a heparin-mimetic binding growth factor with high affinity to heparin and heparin-mimetics, thus, we expect a high encapsulation efficiency of the drug in the NPs.

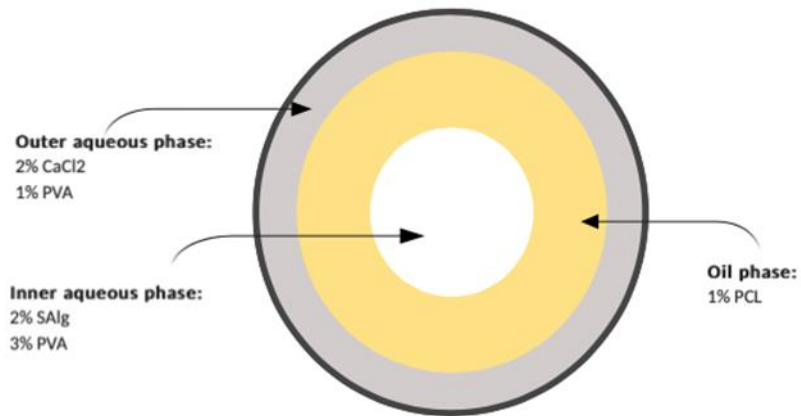


Figure 6. Schematic illustration of AlgSulf/PCL NPs prepared by double emulsion solvent evaporation technique.

Aim 2: Assessment of the nanoparticles' biocompatibility and cellular uptake.

Hypothesis: The materials used to develop the NPs, AlgSulf, PCL, and PVA, were proven to be biocompatible as previously mentioned in the introduction. Hence, we expect that the NPs will not greatly affect the proliferation and activity of HaCaT cells as we increase their concentration.

Moreover, NPs will be tailored to possess an average size less than 500 nm, thus, they are expected to be taken up by HaCaT cells via endocytosis.

Aim 3: Synthesis and characterization of Alg/PCL nanoparticles with AlgSulf outer shell using double emulsion solvent evaporation technique.

Hypothesis: AlgSulf possesses sequestering properties that can help decrease the inflammation at the wound site. Thus, we hypothesize that using AlgSulf as an outer coating to Alg/PCL NPs encapsulating IGF-1 can help in providing a favored dual activity: protecting and delivering the encapsulated GFs to help close the wound, as well as sequestering inflammatory cytokines *via* the AlgSulf at the outer phase of the NPs.

CHAPTER 4

MATERIALS AND METHODS

4.1. Materials

Sulfated Alginate (DS 2.0 AlgSulf), Sulfated Alginate (DS 0.8 AlgSulf) and Sulfated Alginate (DS 2.6 AlgSulf) were purchased from Innovent, Germany. Sodium Alginate (W201502, Mw 160 KDa, Novamatrix, Norway), Poly (vinyl alcohol) (Mw 13,000-23,., 87%-89% hydrolyzed), Polycaprolactone (average Mn 80,000), Dichloromethane (DCM), Dulbecco's Modified Eagle's Medium (DMEM)- high glucose, Fetal Bovine Serum (FBS), Penicillin-Streptomycin, Trypsin Solution 10X, Tween-20, Bovine Serum Albumin, Sodium Hydroxide (NaOH), Avidin-HRP conjugate, ABTS Liquid Substrate Solution, and Phosphate Buffered Saline 10X were obtained from Sigma, USA. Calcium chloride (CaCl₂, Anhydrous) was bought from Fisher Scientific, USA. Recombinant Human IGF-1 and Human IGF-BP1 Standard ABTS ELISA Kit were obtained from Peprotech, UK. ELISA microplates (Nunc MaxiSorp or Corning) and high-capacity cDNA reverse transcription kit were purchased from Thermofisher Scientific, UK. TRIzol reagent was obtained from Ambion Life Technologies and iTag universal SYBR green super mix from Bio-Rad. Sodium Pyruvate was obtained from Lonza, Switzerland.

4.2. Methods

4.2.1. Synthesis of Alg/PCL and AlgSulf/PCL NPs

Preparation of Solutions

Alg/PCL NPs as well as AlgSulf/PCL NPs were prepared using the double emulsion solvent evaporation technique. Briefly, 40 mg of PCL were dissolved in DCM to form a clear organic solution (O) at a concentration of 10 mg/mL. Sodium Alg or AlgSulf (DS_{0.8} or DS_{2.0}) and PVA were mixed by magnetic stirring in 1 mL double-deionized water (DDW) at a concentration of 1% and 3% by weight, respectively, at 60°C until they dissolved completely and formed the inner aqueous phase (W1). The solution was then filtered through a 220 nm syringe filter (Corning), unless specified otherwise. Another aqueous phase containing PVA and CaCl₂ at 1% and 2% weight, respectively, was prepared in 10 mL DDW to form the other dispersed phase (W2).

Formation of NPs

The NPs were synthesized using the double emulsion solvent evaporation technique illustrated in fig. 7. The primary emulsion (W1/O) was formed by dispersing 1 mL of the sodium alginate for PA NPs and sulfated alginate of (a) DS_{0.8} AlgSulf and (b) DS_{2.0} AlgSulf for AlgSulf NPs and PVA (W1) solution in 4 mL of PCL (O) solution. Then, the mixture was homogenized using ultrasonic homogenizer (Q 700 Sonica) at a frequency of 20 KHz and an amplitude of 50% for 5 minutes. To form the secondary emulsion (W1/O/W2), the second aqueous phase containing PVA and CaCl₂ (W2) was added dropwise into the primary emulsion. This mixture was homogenized at an amplitude of 65% for 10 minutes. The double emulsion was then left on the stirrer for a minimum of 3 hours for the organic solvent to evaporate in a container with a

surface area of 2463 mm² at room temperature and atmospheric pressure. Afterwards, the particles were collected by centrifugation at a speed of 14,800 RPM for 20 minutes at 4°C and washed with DDW to remove any PVA or DCM residues. Then the particles were placed at -80°C for a minimum of 30 minutes to be later dried in the lyophilizer (Labconco) for 48 hours. When freeze-dried, the particles can be stored at 4°C for up to year.

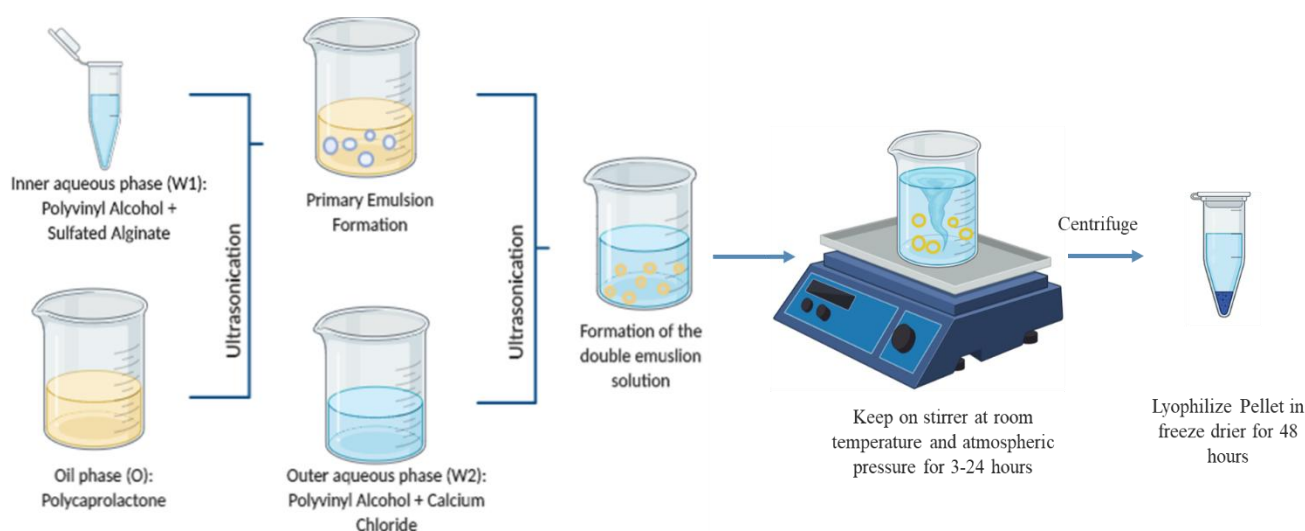


Figure 7. Schematic illustration of AlgSulf/PCL NPs formation using the double emulsion solvent evaporation technique.

4.2.2. Physical Characterization of the NPs

4.2.2.1. Average Hydrodynamic Size and Zeta Potential

After synthesizing the particles, their average hydrodynamic diameter, polydispersity index (PDI), and zeta potential were measured by dynamic light scattering using NanoPlus HD[®] DLS. The samples were prepared by adding 10 µL of particulate dispersion to 990 µL DDW and then placed in a plastic cell to be analyzed at

25°C. As for the zeta potential, the samples were prepared in a similar manner and then inserted into a flow cell for analysis.

4.2.2.2. Morphology

The morphology of the NPs was analyzed using the scanning electron microscopy (SEM) by “MIRA 3 TESCAN”. The freeze-dried NPs were mounted on metallic stubs using double sided adhesive carbon tabs. The NPs were then sputter coated with a 20 nm thick layer of gold, chromium, platinum, or any other conductive metal using Quorum 150 V Plus. Images of the samples were then taken using the SEM.

4.2.3. Encapsulation and Release of IGF-1 from Nanoparticles

NPs preparation

Two concentrations of IGF-1 (250 ng/mL and 1000 ng/mL) were encapsulated in AlgSulf/PCL NPs and Alg/PCL NPs by adding adequate IGF-1 concentration in the inner aqueous phase W1 after filtration. After obtaining the final mixture (W1/O/W2) following the steps mentioned in section 1.2.

Encapsulation and Loading Capacity of IGF-1

The NPs suspension was centrifuged at 4°C and 14,800 RPM for 20 minutes, and then the collected particles were washed by DDW. The amount of IGF-1 loaded into the nanoparticles was calculated as the difference between the total IGF-1 used to prepare the initial mixture and the amount that was found in the supernatant. The amount of IGF-1 was quantified by using enzyme linked immunosorbent assay

(ELISA). The encapsulation efficiency (% EE) was determined in duplicates using the following formula:

$$\% EE = \frac{\text{Total IGF1} - \text{Free IGF1}}{\text{Total IGF1}} \times 100$$

The loading capacity of the NPs was determined in duplicates using the following formula:

$$\% LC = \frac{\text{Encapsulated IGF1}}{\text{Mass of NPs}} \times 100$$

Release Rate of IGF-1

In vitro release profile of IGF-1 from NPs was determined as follows. The IGF-1 loaded Alg/PCL and AlgSulf/PCL NPs were prepared as mentioned earlier in section 3.1. After the centrifugation (at 4°C and 14,800 RPM for 20 minutes) and washing in DDW, the NPs were then freeze dried. A 10 mg quantity of the dried Alg/PCL and AlgSulf/PCL NPs were then re-dispersed into 1 mL of PBS (pH 7.2) in Eppendorf tubes and placed at 37°C under continuous stirring conditions (200 RPM). At different time intervals (0, 1, 2, 4, 24, 48, 168, and 336 hours), the samples were centrifuged at 14,800 RPM for 30 minutes and the 1 mL supernatants were collected, and 1 mL of fresh PBS was added to each Eppendorf tube. The Eppendorf tubes were then placed back at same conditions.

All removed supernatants were stored at -20°C until quantified. The amount of IGF-1 in the supernatant was calculated using the ELISA assay. A control consisting of the supernatant collected from NPs without encapsulated IGF-1 was used to correct for

the effect of NPs degradation on the assay. The cumulative release rate was then obtained by adding up the IGF-1 amount released at each time point to the IGF-1 released during the previous time interval then divided by the IGF-1 that was initially added to the NPs.

The release rate (RR) was calculated using the following equation:

$$\%RR = \frac{\text{Cumulative IGF1 released}}{\text{Encapsulated IGF1}} \times 100$$

4.2.4. Cytotoxicity of NPs

Cell Culture

The HaCaT human keratinocyte cell line was used to perform the *in vitro* experiments. The cells were cultured in DMEM-high glucose supplemented with 10 % FBS, 1 % sodium pyruvate, 1 % penicillin-streptomycin, 0.2 % kanamycin at 37°C and 5 % CO₂. The cells were cultured in T-75 flasks and sub-cultured when they reached 100 % confluency. Cells were prepared for experiments by discarding the medium, then washing them with PBS to remove any traces of medium. Trypsin-EDTA solution was added to cover the whole surface of the flask. Then the flasks were incubated for 10 minutes at 37°C to allow cells to detach completely. A minimum amount of about double the trypsin volume of complete medium was added to deactivate trypsin, after which the mixture was collected in a 15 mL conical tube. The cells were collected by centrifugation at 1200 RPM for 5 minutes to be counted. Accordingly, the cells were prepared with cell culture medium at the desired density to be seeded in 6, 12, or 96-well plates depending on the experiment to be done.

MTT Assay

The MTT (3-(4,5-dimethylthiazolyl-2)-2,5-diphenyltetrazolium bromide) assay is used to evaluate the cells' proliferation rate. The MTT yellow tetrazolium salt is reduced by mitochondrial dehydrogenases to the water insoluble purple blue formazan compound in metabolically active and viable cells, while apoptotic and necrotic cells with low metabolic activity do not convert MTT to Formazan [93].

As shown in fig. 8, HaCaT cells were seeded at a density of 50,000 cells/well in a 96-well plate, in triplicates, and exposed to different concentrations of AlgSulf_{2.0}/PCL NPs (0, 2.6, 13, 26, and 53 µg/cm²). At 40-50% confluency, the media was aspirated and replaced with NPs-containing media. After incubating the cells with NPs for 24 hours, 90 µL of fresh media and 10 µL of the MTT solution were added to each well. The cells were left to react with MTT for 3 hours in dark at 37°C until dark purple formazan crystals were formed. These crystals were then solubilized by adding to each well 150 µL of the MTT stop solution containing the organic iso-propanol solvent, triton X-100, and 37% HCl. The solutions were then transferred into a new plate to disregard the effect of any sediment particles. The plate was then read at a 595 nm absorbance spectrophotometrically using a microplate reader. A well containing cells treated with 0 µg/mL NPs was used as a control reference for this experiment representing 100% activity. To determine the % activity, the following formula was used:

$$\% \text{ Activity} = \frac{OD \text{ treated cells} - OD \text{ blank}}{OD \text{ control} - OD \text{ blank}} \times 100$$

The experiment was repeated three times.

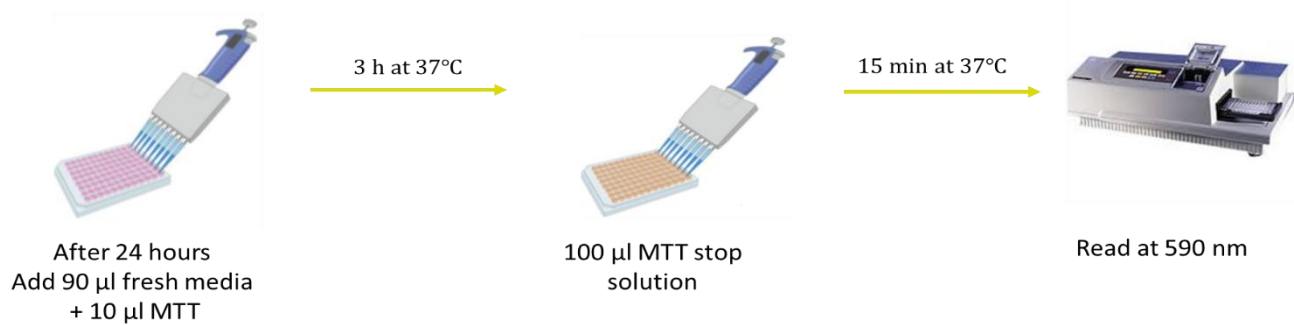


Figure 8. Schematic of the MTT Assay.

Trypan Blue Exclusion Assay

As illustrated in fig. 9, HaCaT cells were seeded at a density of 50,000 cells/well in a 24-well plate. The cells were cultured in DMEM-high glucose media until they became 40-50% confluent. Then, the culture media was aspirated and replaced by fresh media containing AlgSulf_{2.0}/PCL NPs at the following concentrations: 0, 5, 25, 50, and 100 µg/mL. The cells were incubated in the media containing NPs for 24, 48, and 72 hours. At each time point, trypsin was added to detach the cells, then the pellet collected by centrifugation was stained with trypan blue (1:1 dilution in media). Trypan blue dye gets absorbed by dead cells that have a porous membrane. The amount of the viable cells at each condition is then calculated via the following formula:

$$\% \text{ viability} = \frac{\text{number of viable cells}}{\text{number of viable cells} + \text{number of dead cells}} \times 100$$

The percentage viability is then obtained after normalizing the results at each condition against the 0 µg/mL condition.

All samples were done in triplicates.

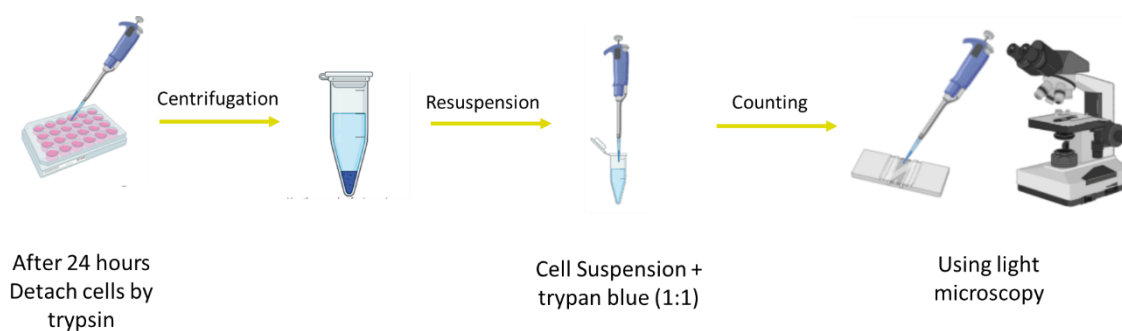


Figure 9. Schematic representation of the Trypan Blue exclusion Assay.

For the MTT assay and trypan blue exclusion assay, the concentrations of the NPs added to the wells were adjusted according to the wells' surface area because NPs manage to settle as time passes [94]. The surface area of the 24-well plate is 1.9 cm²/well, and that of the 96-well plate is 0.32 cm²/well. The concentrations' modifications are present in table 1:

NPs' concentration in 24-well plate ($\mu\text{g/mL}$)	5	25	50	100
NPs' concentration in 96-well plate ($\mu\text{g/cm}^2$)	2.6	13	26	53

Table 1. Treatment concentrations conversion from $\mu\text{g/mL}$ to $\mu\text{g/cm}^2$.

4.2.5. Cellular Uptake of Nanoparticles

Cellular uptake of Alg/PCL NPs and AlgSulf/PCL NPs was quantified by fluorescence intensity using Tristar multimode microplate reader. HaCaT cells were seeded in 96-well plates at a concentration of 50,000 cells/well. The NPs were prepared using FITC labeled Alg or AlgSulf to allow fluorescent labeling of the NPs, following the same synthesis technique described in section 1.2. After synthesizing and freeze-

drying the FITC-labeled NPs, 100 µg/mL of DMEM-high glucose FITC-Alg/PCL and FITC-AlgSulf/PCL NPs were sonicated for 1 minute and sterilized in the culture- hood for at least 40 minutes under UV-light. After 24 hours of cells' incubation, media was discarded from wells and cells washed with 1X PBS (without Ca²⁺ and Mg²⁺). Next, NPs were added onto the cells in DMEM-high glucose at 37°C and plates were cultured for a predetermined time of 1,2, and 4 hours. For excitation of FITC fluorescence, an argon laser with an excitation wavelength of 488 nm was used and the emission wavelength was 515 nm. The media within each well was transferred to new wells to measure the fluorescence intensity of FITC-labeled Alg NPs that were not taken up by cells. The fluorescence intensity of FITC-labeled Alg NPs taken by the HaCaT cells was quantified with the fluorescence microplate reader after cytolysis with 0.5% Triton X-100 for 15 min.

The experiment was done in triplicates, and the cellular uptake efficiency was calculated using the following equation:

$$\text{Cellular Uptake (\%)} = \frac{\text{Fluorescence of NPs in cells}}{\text{Fluorescence of NPs in media} + \text{Fluorescence of NPs in cells}} \times 100$$

4.2.6. Enzyme Linked Immunosorbent Assay (ELISA)

To detect and quantify IGF-1 released by the NPs, human IGF-BP1 standard ABTS ELISA Sandwich Kit was used according to the manufacturer's instructions. Briefly, the capture antibody (250X) was diluted to 1X in PBS. The ELISA plate was then coated with 100 µL/well of the diluted polyclonal capture antibody, sealed and placed at room temperature overnight. Around 24 hours later, the plate was washed 4

times using a wash buffer (0.05% Tween-20 in PBS 1X). Then, 300 μL of ELISA blocking buffer (1% BSA in PBS 1X) were pipetted into each well and incubated for an hour at room temperature. Meanwhile, serial dilution of the standards from 1500 pg/mL to 11.7187 pg/mL was conducted using the diluted ELISA diluent (0.05% Tween-20, 0.1% BSA in PBS 1X) as illustrated in Fig.7. After the blocking step, the plate was washed 4 times then 100 μL of the standards and samples were pipetted to each well in technical duplicates.

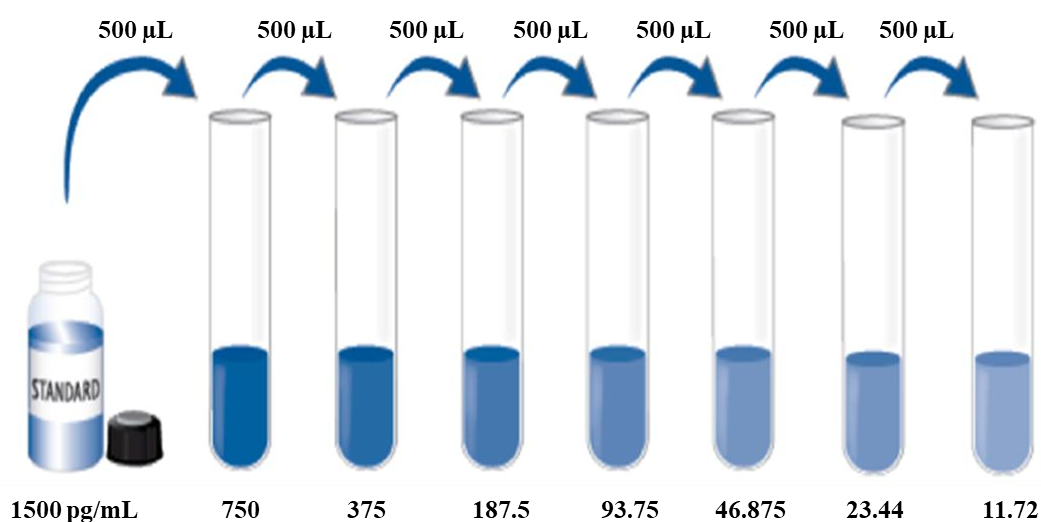


Figure 10. Serial dilutions of ELISA standard (pg/mL).

Two wells served as blanks where 100 μL of the diluent were added. The plate was then incubated for 2 hours at room temperature. After washing 4 times, 100 μL of the detection antibody diluted from 250X to 1X in ELISA diluent were added to each well followed by an incubation period of 2 hours at room temperature. After additional washing, 100 μL of the avidin horseradish peroxidase (avidin-HRP conjugate), diluted

from 250X to 1X in ELISA diluent, were added to each well. The plate was then sealed and incubated for half an hour at room temperature. Finally, 100 μ L of ABTS Liquid ELISA substrate were added into each well in the dark, after washing the plate for 4 times. The plate was then enfolded with aluminum foil and placed at room temperature until color development. The color development was monitored using an ELISA microplate reader at 405 nm with a wavelength correction at 650 nm. The plate was read every 5 minutes for 40 minutes until the optical density (O.D.) values no longer changed.

4.2.7. AlgSulf-coated Alg/PCL NPs as scavengers of inflammatory cytokines

NPs formation

The NPs formation process was performed as previously mentioned in section 2.1. After centrifugation, the pellet containing the Alg/PCL NPs was obtained. Then, it was dissolved in 5 mL of 1% DS_{2.0}AlgSulf, the mixture was then sonicated for 1 minute to ensure their even distribution in the beaker, then left overnight on the stirrer at room temperature. Then the mixture was centrifuged at a speed of 14,800 RPM for 20 minutes at 4°C. The pellet was now placed in a 2% CaCl₂ solution, sonicated for 1 minute, then left on a stirrer for 2 hours to allow AlgSulf crosslinking with the outer phase of NPs. A final centrifugation was done using the same parameters as previously mentioned, the pellet was then stored at -80°C for a minimum of 30 minutes, and then dried in the lyophilizer (Labconco) for 48 hours. When freeze-dried, the particles can be stored at 4°C for up to year.

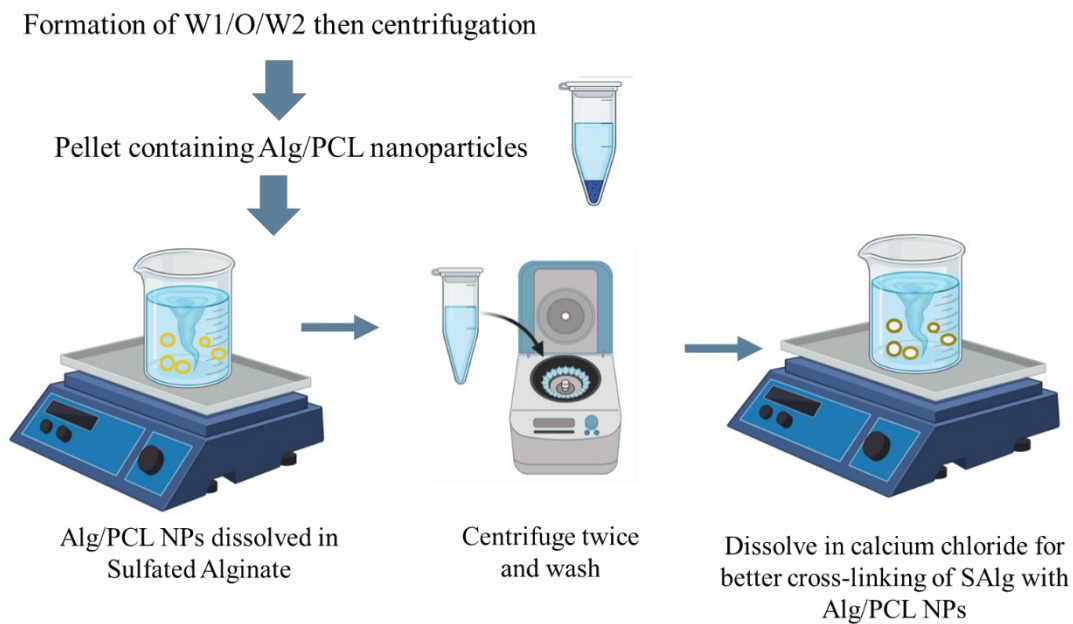


Figure 11. Schematic illustration of AlgSulf coating on the Alg/PCL NPs.

4.2.8. AlgSulf-coated Alg/PCL NPs Characterization

4.2.8.1. Average Hydrodynamic Size and Zeta-Potential

After synthesizing the particles, they were characterized for their average hydrodynamic diameter, polydispersity index (PDI), and zeta potential using the dynamic light scattering using Nano Plus HD[®] DLS. For this purpose, the NP samples were diluted in DDW by adding 10 μL of NPs to 990 μL DDW.

4.2.8.2. Morphology

The morphology of the synthesized AlgSulf-coated Alg/PCL NPs was analyzed using the “MIRA 3 TESCAN” SEM. The freeze-dried NPs were prepared following the same procedure described in section 2.2. Then images of the samples were taken using the SEM at different magnifications.

4.2.8.3. Fourier transform infrared spectroscopy (FTIR)

FTIR spectra of AlgSulf-coated Alg/PCL NPs were obtained using an infrared spectrophotometer from Agilent technologies. A small thin layer of the NPs was placed at the machine's disk where an infrared beam was directed at the sample.

4.2.9. NPs effect on inflammation

HaCaT cells were seeded in 12-well plates at a density of 1,000,000 cells/well in a high glucose complete DMEM medium and cultured at 37°C until they formed a confluent monolayer. The cells were seeded in 11 wells for these 11 conditions: (1) cells without LPS (negative control), (2) cells + LPS (positive control), (3) AlgSulf-coated Alg/PCL NPs treated cells + LPS, (4) 2% AlgSulf_{2.0}/PCL NPs treated cells + LPS, (5) 2% Alg/PCL NPs treated cells + LPS, (6) IGF-1 loaded- AlgSulf-coated Alg/PCL NPs treated cells + LPS, (7) IGF-1 loaded 2% DS2.0AlgSulf/PCL NPs treated cells + LPS, and (8) 2% Alg/PCL NPs treated cells, (9) Alg + LPS, (10) AlgSulf + PCL, (11) IGF-1 + LPS. After 24 hours, media was discarded, and the wells were washed with PBS to remove any floating cells. Then, 100 µg/mL of the treatments were added to wells (3-11) while fresh serum free DMEM-high glucose was added to the control wells. To prepare the treatments, 1 mg of each NPs formation was added to 10 mL complete DMEM media and placed under UV light for a minimum of 20 minutes to allow their sterilization. After 24 hours of treatment, the supernatants were collected in Eppendorf tubes and stored at -20°C for ELISA assay and the cells were collected for RNA extraction for qRT-PCR. This experiment was performed in triplicates.

4.2.10. Quantitative Real Time Polymerase Chain Reaction (qRT-PCR)

The differential expression levels of human interleukin-6 (H-IL-6) and human tumor necrosis factor alpha (H-TNF- α) were evaluated using qRT-PCR analysis.

RNA extraction

After 24 hours of treating the HaCaT cells with LPS in high glucose medium to mimic diabetic wound conditions, the total RNA was extracted from cells using TRIzol™ Reagent (Ambion; Life Technologies), following the manufacturer's protocol. All steps were performed on ice. First, we collected the 1 mL DMEM media from each well in the 12-well plate and transferred them into Eppendorf tubes. The tubes were then stored at -20°C, to further perform ELISA Assay. The cells in the wells were washed with PBS (without Ca²⁺/Mg²⁺), which was then aspirated. Then, 500 μ L of TRIzol™ Reagent was added to each well and they were scraped thoroughly. The cell lysates were transferred into Eppendorf tubes that were vortexed for 30 seconds. To allow the homogeneity of the tubes' content, 100 μ L of chloroform were pipetted into each tube, they were then vortexed. The tubes were incubated for 5 minutes at room temperature, then centrifuged for 15 minutes at 12,000g at 4°C. The aqueous phases, that constitutes the RNA, were pipetted, and transferred into new Eppendorf tubes, where 200 μ L of isopropanol was added to allow their precipitation. The tubes were then vortexed for 15 seconds and left at room temperature for 10 minutes. All samples were centrifuged again for 15 minutes at 12,000g at 4°C forming white gel-like pellets (RNA). The supernatants were discarded and 400 μ L of 75% ethanol was added to each tube, followed by centrifugation for 5 minutes at 7,500g at 4°C. The supernatants were later discarded, and again the pellet was centrifuged for 5 minutes at 7,500g at 4°C. To

confirm the removal of all ethanol traces, the tubes were left to dry under the hoods for 15 minutes at room temperature. In the end, 20 μL of DNase/RNase-free water was added to the RNA samples, and the tubes were placed for 5 minutes at 60°C. To assess the purity and concentration of the RNA extracted, the samples were put on ice and the absorbance of 1 μL of each sample was measured using the DeNovix DS-11FX. Lastly, RNA should be stored at -80°C before performing PCR.

Reverse transcription of RNA to cDNA

The first step is the reverse transcription of RNA into complementary DNA (cDNA). Specifically, cells were washed with PBS 1X, then 500 μL TRIzol reagents were added to each well and cells were scraped and collected in Eppendorf tubes for RNA extraction, Nanodrop 2000 was used to determine the concentration and the purity of the total RNA. Then, using the High-Capacity cDNA Reverse Transcription Kit (Applied Biosystems by Thermo Fischer Scientific) and following the manufacturer's protocol, the RNA samples were reverse transcribed to cDNA. Before keeping the tubes on ice while working, they were centrifuged to suspend the whole amount including any residues from the tube's sides. Then, RNase-free water was added to 1 μg of each RNA sample to get a total volume of 14.2 μL (H_2O and RNA). Then, the reverse-transcription reaction was performed by preparing a master mix containing the following components per one reaction: 2 μL RT buffer, 2 μL RT Random Primers, 1 μL MultiScribeTM Reverse Transcriptase, and 0.8 μL dNTP Mix. The total volume for RT-PCR should be 20 μL , so 5.8 μL of the RT (reverse transcription) mix volume was transferred into each tube of template RNA, then mixed gently. The tubes were then briefly centrifuged and placed in the Thermal Cycler T100 Biorad machine for 2 hours and 17 minutes. Finally,

30 μ L RNase-free water were added to each Eppendorf to dilute the cDNA and get a final volume of 50 μ L.

Quantitative polymerase chain reaction (qPCR)

The primer oligonucleotide sequences (table 2) were manufactured from Macrogen. To analyze the results, Glyceraldehyde-3-Phosphate Dehydrogenase (GAPDH) housekeeping gene was used for normalization as a reference gene. All the primer tubes were centrifuged at 1,000 RPM for 1 minute to obtain all lyophilized products as pellets.

Gene	Forward Primer	Reverse Primer
GAPDH	5'- GAAGGTGAAGGTCGGAGTC -3'	5'- GAAGATGGTGATGGGATTTC -3'
IL-6	5'- CTTCGGTCCAGTTGCCTTCT -3'	5'- GAGATGCCGTCGAGGATGTA -3'
TNF- α	5'- CAGAGGGCCTGTACCTCATC -3'	5'- GGAAGACCCCTCCAGATAG -3'

Table 2. Forward and reverse primer sequences used for RT-PCR.

Then, 300 μ L of DNase/RNase free water was added to each tube to get the stock concentration of 100 μ M. The tubes were then vortexed and centrifuged at 1,000 RPM for 1 minute. To obtain the working concentration of 50 μ M, 10 μ L from each stock was dissolved in 10 μ L RNase-free water. The iTaqTM Universal SYBR[®] Green Supermix, primers, and DNA samples were placed on ice, then mixed thoroughly and centrifuged briefly to collect solutions in the bottom layer of the tubes. For each transcript reaction, a master mix was prepared on ice according to the following volumes: 5 μ L iTaqTM Universal SYBR[®] Green Supermix, 2.3 μ L DNase/RNase free

water, and 0.1 μ L forward and reverse primers. The mixtures were then mixed well and spun down to ensure homogeneity, and 7.5 μ L of the master mix was loaded into each reaction well of a 384-well PCR BioRad plate. Then, 2.5 μ L of cDNA was added to the wells. Since a no-template control was included in each plate reaction, 2.5 μ L of DNase/RNase free water was added instead of cDNA. Finally, the PCR plate was sealed using an adhesive sealer and aluminum foil, centrifuged at 1,100 RPM for 1 minute and loaded into the Real-Time PCR BioRad CFX384 machine. The qRT-PCR thermal cycling conditions which included a melt curve to verify the specificity of the product were applied as per Table 3.

Step	Temperature	Time
Polymerase Activation	95 °C	5 mins
Denaturation	95 °C	10 secs
Annealing	60 °C	30 secs
Extension	72 °C	30 secs
Melt Curve		5 secs

Table 3. Different steps of RT-PCR.

All the following qRT-PCR experiments were conducted in biological triplicates under sterile conditions, using filtered tips and molecular grade nuclease-free water.

4.3. Statistical Analysis

All statistical tests were performed using GraphPad software. When comparing two groups, independent t-test was used for parametric data and Mann–Whitney U test for non-parametric data. When comparing more than two groups, One-Way ANOVA was used for parametric data and Kruskal Wallis for non-parametric data. Two-Way ANOVA was used when groups were studied against two variables. A p-value of less than 0.05 was considered significant (*).

CHAPTER 5

RESULTS AND DISCUSSION

5.1. Characterization and morphology of AlgSulf/PCL NPs

The preparation of NPs was based on the double emulsion solvent evaporation technique and dissolving AlgSulf with different degrees of sulfation (0, 0.8, 2.0, and 2.6) in the inner aqueous phase. The 0 degree of sulfation refers to non-sulfated pure sodium alginate that is used as a reference. Our results indicated that using AlgSulf_{2.0} in the inner aqueous phase of NPs resulted in a smaller average size of NPs in comparison to pure Alg, AlgSulf_{0.8}, and AlgSulf_{2.6}. Importantly, when compared to pure Alg, the three AlgSulf NPs samples had a smaller size. As illustrated in Fig. 12, the size of NPs, measured by DLS, is affected by the DS of the Alg dissolved in the inner aqueous phase. The AlgSulf_{0.0}/PCL, AlgSulf_{0.8}/PCL, AlgSulf_{2.0}/PCL, and AlgSulf_{2.6}/PCL NP's size are 360 ± 18.67 , 246 ± 15.47 , 221 ± 8.9 , and 300 ± 10.24 nm, respectively. Thus, all these NPs present a size that is within the desired range (100-300 nm).

Importantly, NPs prepared by dissolving AlgSulf_{2.0} in the inner aqueous phase have the smallest size when compared to other samples. The decreasing trend in the NPs' size could be attributed to the weaker cross-linking between the positively charged Ca²⁺ ions and the negatively charged sulfate and hydroxyl groups in the AlgSulf_{0.8} and AlgSulf_{2.0} compared to the more abundant crosslinking between the positively charged Ca²⁺ ions and negatively charged hydroxyl groups in AlgSulf_{0.0}. Furthermore, this

decrease in size could be attributed to the lower storage modulus of AlgSulf_{2.0} resulting from the introduced sulfate groups that cause a lower crosslinking density [95].

The NPs with size between 100 and 500 nm is desired since NPs with size less than 100 nm are quickly eliminated from the circulation via the reticuloendothelial system and NPs larger than 500 nm are less likely to be taken up by cells [96]. In addition, the size of NPs is within the optimal size range to achieve efficient biodistribution and maximal residence time where 60% of the particles can be retained within the tissue. Outside this size range, around 20% of NPs remain in the circulation, and thus are more prone to be cleared out by the body [97].

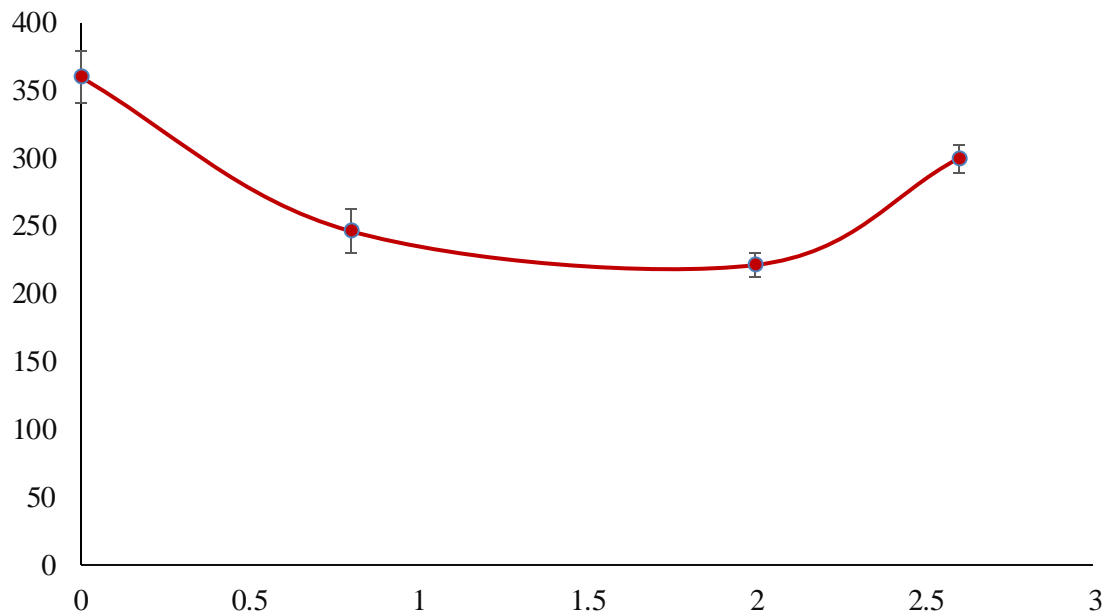


Figure 12. Effect of the degree of sulfation of AlgSulf in the inner aqueous phase of the NPs on their average hydrodynamic size. The size was measured by DLS. $p=0.0018$ as shown by one-way ANOVA. Tukey post hoc's test shows significant difference (** $p < 0.01$) between AlgSulf_{2.0}/PCL and AlgSulf_{0.0}/PCL and between AlgSulf_{0.8}/PCL and AlgSulf_{0.0}/PCL NPs. The data is reported as mean \pm SEM (n=3).

Importantly, the increase in DS of AlgSulf up to 2.6 had a deteriorating effect on its gelling ability resulting in decreased stiffness. As we increase the DS to 2.6, the cross-linking between AlgSulf becomes only transient and leads to formation of unstable NPs, which induces their agglomeration and forms larger AlgSulf_{2.6}/PCL NPs [90]. In addition, we measured the NPs' zeta potential by DLS as it determines the surface charge of the NPs and their colloidal stability. Values between ± 0 and 10 mV refer to unstable NPs while ± 10 and 30 mV refers to stable NPs and ± 30 mV refers to highly stable NPs [98]. The values obtained, as shown in Fig. 13, were all negative due to the presence of the negative charge of Alg, AlgSulf, and PCL. The values obtained were -11.1 ± 0.78 , -11.3 ± 1.08 , -15.6 ± 1.78 , and -6.7 ± 0.68 mV for AlgSulf_{0.0}/PCL, AlgSulf_{0.8}/PCL, AlgSulf_{2.0}/PCL, and AlgSulf_{2.6}/PCL NPs, respectively. The values show good colloidal stability as they range between -10 and -20 mV for all samples except the AlgSulf_{2.6}/PCL NPs. This indicates that the NPs can repel each other due to their surface charge and as such this decreases the risk of aggregation resulting in bigger sized particles. The results presented in Fig. 13 show significantly different zeta potential values ($p=0.004$) showing that the DS of alginates can influence the surface charge of the NPs. This can be attributed to the more negative sulfate groups of AlgSulf as compared to the lower negatively charged carboxyl groups present in pure alginate [90].

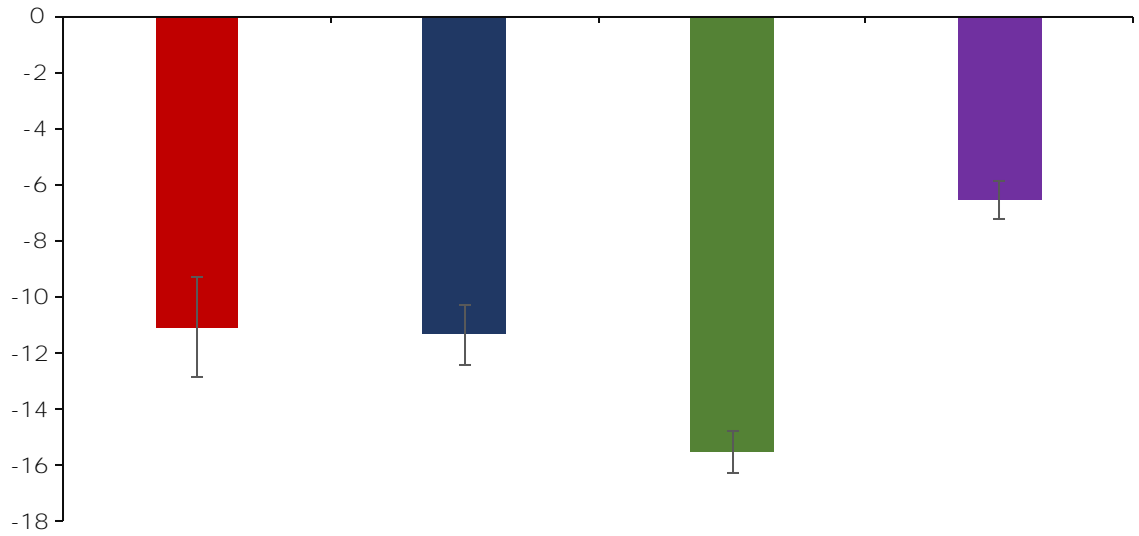


Figure 13. Effect of the degree of sulfation of AlgSulf in the inner aqueous phase of the NPs and their zeta potential. The zeta potential was measured by DLS. $p=0.004$ as shown by one-way ANOVA test. Tukey post hoc's test shows significant difference ($*p < 0.05$) between the AlgSulf_{2,0}/PCL and control AlgSulf_{0,0}/PCL NPs and AlgSulf_{2,6}/PCL and control AlgSulf_{0,0}/PCL NPs. The data is reported as mean \pm SEM (n=3).

Zeta-potential is not measured directly by DLS, rather it is deduced from the electrophoretic mobility of the charged particles under an applied electric field [99]. The zeta is then calculated through the following equation:

$$\zeta = \frac{\mu \eta}{\epsilon_r \epsilon_0}$$

Where:

ζ is the zeta potential

μ is the electrophoretic mobility

η is the viscosity

ϵ_r is the relative permittivity/dielectric constant

ϵ_0 is the permittivity of vacuum

From the mentioned equation, we can notice that the zeta potential of NPs is directly related to their mobility. Thus, as we go from 2.0 to 2.6 DS of AlgSulf in the inner phase of NPs, the size increases which decreases the mobility and consequently leads to a decrease in the absolute value zeta potential.

Polydispersity index (PDI) is a parameter that indicates the size distribution of the NPs. The results show that the PDI values for the NPs were 0.161 ± 0.01 , 0.129 ± 0.007 , 0.113 ± 0.0069 , and 0.229 ± 0.0228 for AlgSulf_{0.0}/PCL, AlgSulf_{0.8}/PCL, AlgSulf_{2.0}/PCL, and AlgSulf_{2.6}/PCL NPs, respectively. These results indicate that AlgSulf_{2.0}/PCL NPs have a more homogeneous distribution of their size compared to other samples as they have the smallest PDI value. The optimal value of PDI is close to zero and is linked to a monodisperse sample especially when the PDI value is <0.3 , indicating a homogeneous distribution of the NPs size. Values that are closer to 1 are associated with a polymodal size distribution of the NPs sample [97]. The advantage behind using the double emulsion solvent evaporation technique is to be able to control the size, PDI, and zeta potential to achieve desired drug encapsulation and release [100].

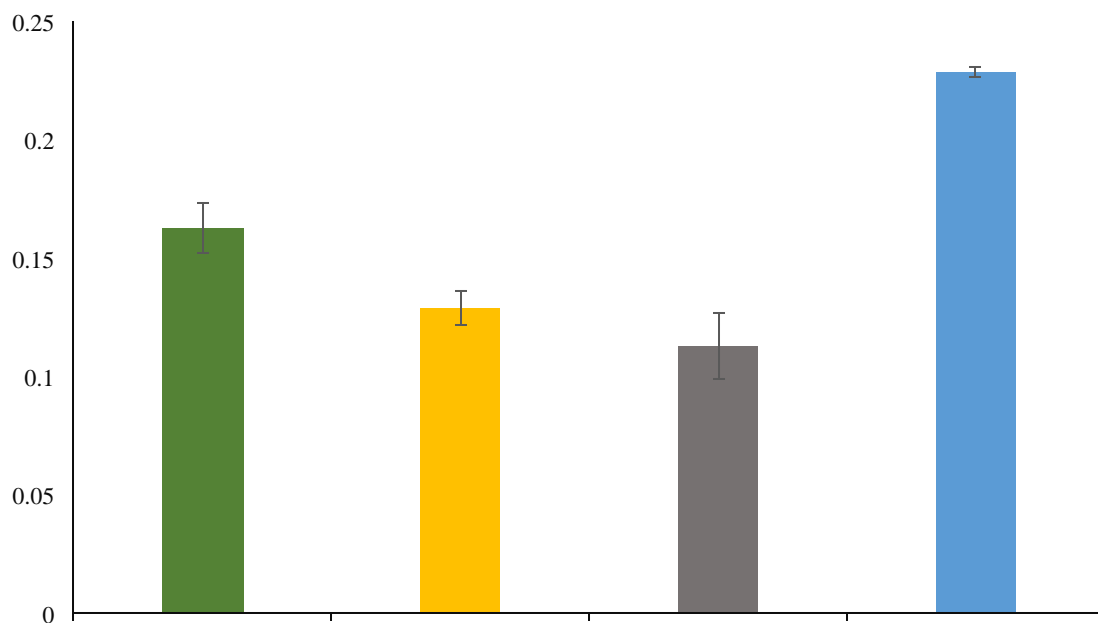


Figure 14. Effect of the degree of sulfation of AlgSulf in the inner aqueous phase of the NPs on the PDI of the particles. $p=0.0007$ as shown by one-way ANOVA test. Tukey post hoc's test shows significant difference ($*p < 0.05$) between AlgSulf_{2,6}/PCL NPs and the control AlgSulf_{0,0}/PCL NP. The PDI was measured by DLS. The data is reported as mean \pm SEM (n=3).

Morphology of the NPs was analyzed using SEM and images are shown in Fig. 15. The NPs appear to be distinct, spherical particles with a smooth surface structure, mainly due to the crosslinking of AlgSulf and Alg with Ca^{2+} ions (fig. 15 a-c) [101]. Figure 15-d shows a more disrupted morphology rather than spherical well shaped NPs which is linked to the transient crosslinking between AlgSulf_{2,6} that increases the NPs' swelling.

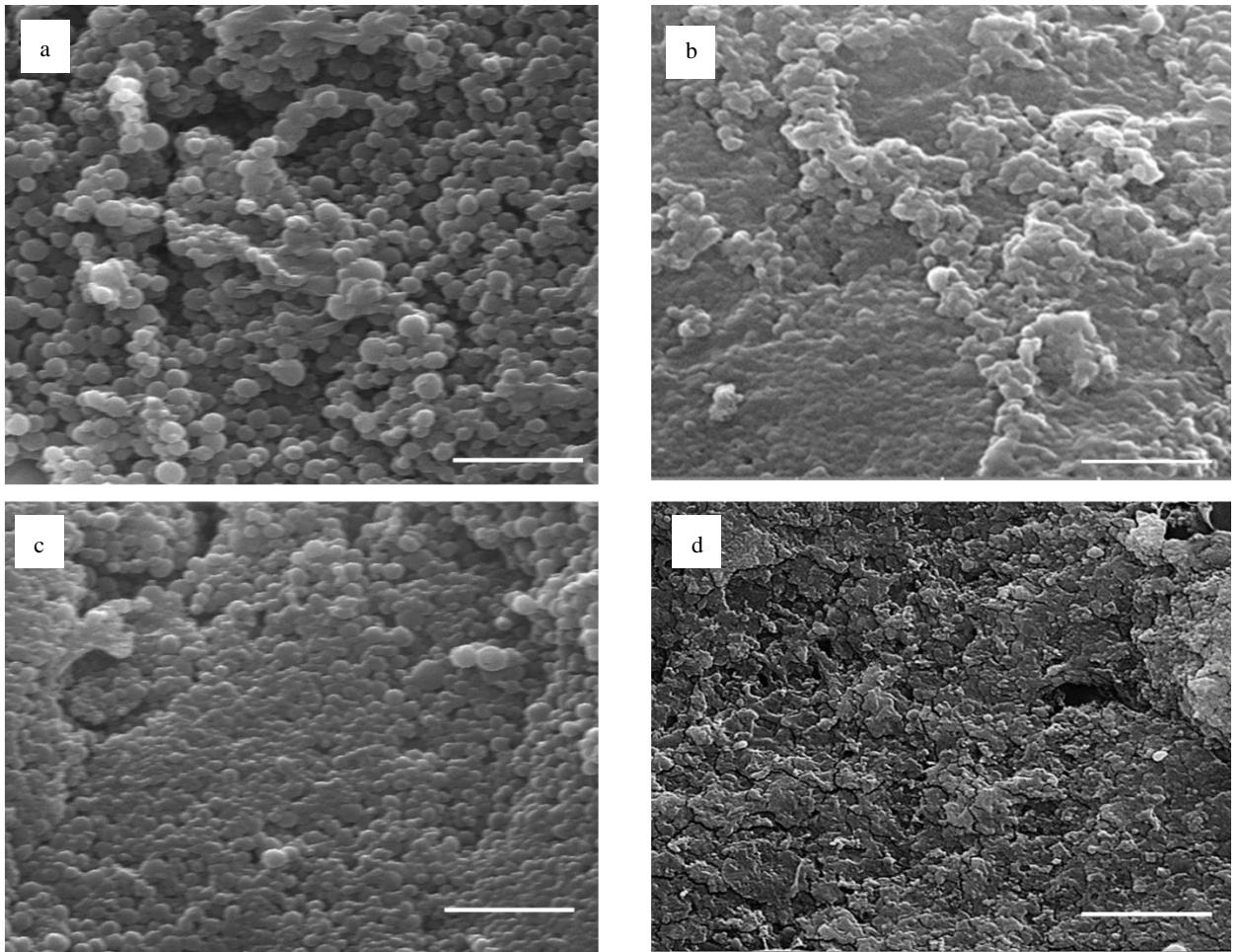


Figure 15. SEM images of NPs. (a) AlgSulf0/PCL NPs (b) AlgSulf0.8/PCL NPs (c) AlgSulf2.0/PCL NPs (d) AlgSulf2.6/PCL NPs. Scale bar = 5µm.

5.2. IGF-1 Encapsulation Efficiency

The optimal formulation for drug encapsulation was studied by analyzing the physicochemical properties of the different formulations of NPs loaded with IGF-1. This was done by observing the particle size (nm), PDI, and zeta potential (mV) as presented in table 4. In addition, the encapsulation efficiency (EE %) and loading capacity (LC %) were determined by ELISA and are illustrated in Fig. 16 and 17, respectively. Dissolving AlgSulf_{2.0} and AlgSulf_{0.8} instead of AlgSulf_{0.0} in the inner aqueous phase of NPs loaded with 1000 ng/mL IGF-1 slightly increased the EE % from

95.56 % \pm 1.89 for pure AlgSulf_{0,0} to 98.59 % \pm 0.48 and 97.43 % \pm 2.83 for AlgSulf_{0,8} and AlgSulf_{2,0}, respectively. This can be related to the higher binding affinity of heparin-mimetic AlgSulf to IGF-1 compared to Alg. Also, it is known that the viscosity of the inner phase of the NPs affects the EE %, thus, we believe that AlgSulf leads to an increase in EE % due to a lower Young's modulus compared to AlgSulf_{0,0} [89].

In a previous study, Wei et al. demonstrated that the encapsulation of IGF-1 in double emulsion PLGA NPs reached 61.26 \pm 2.71 % [102]. Another study performed by Hameed et al. showed that PLGA NPs can entrap 67 \pm 2 % of IGF-1 [103]. When comparing the results of these studies to those obtained in this project, we find a higher EE% of IGF-1 in AlgSulf/PCL NPs. This could be due to the amorphous structure of PLGA compared to a more crystalline PCL structure allowing higher entrapment of IGF-1.

The NPs also presented a low LC % of 2.68 \pm 0.19, 3.08 \pm 0.22, and 5.12 \pm 0.17 for AlgSulf_{0,0}/PCL, AlgSulf_{0,8}/PCL, and AlgSulf_{2,0}/PCL NPs, respectively, which is attributed to the very small amount of IGF-1 (1000 ng/ml) added to the mixture. A higher LC % of IGF-1 is ideally preferable, because even in the case of biodegradable and biocompatible NPs, the presence of unreasonably high quantity of the drug carrier NPs can lead to toxicity problems [104].

Samples	Size (nm)	Zeta Potential (mV)	PDI
IGF-1 loaded Alg/PCL NPs	324 ± 18	-9.7 ± 2.1	0.12 ± 0.02
IGF-1 loaded AlgSulf _{0.8} /PCL NPs	265 ± 21	-11.41 ± 3.5	0.203 ± 0.003
IGF-1 loaded AlgSulf _{2.0} /PCL NPs	243 ± 11.5	-14.61 ± 4.6	0.156 ± 0.019

Table 4. Characteristics of IGF-1 loaded NPs in terms of size, PDI, and zeta potential. The data is reported as mean ± SEM (n=2).

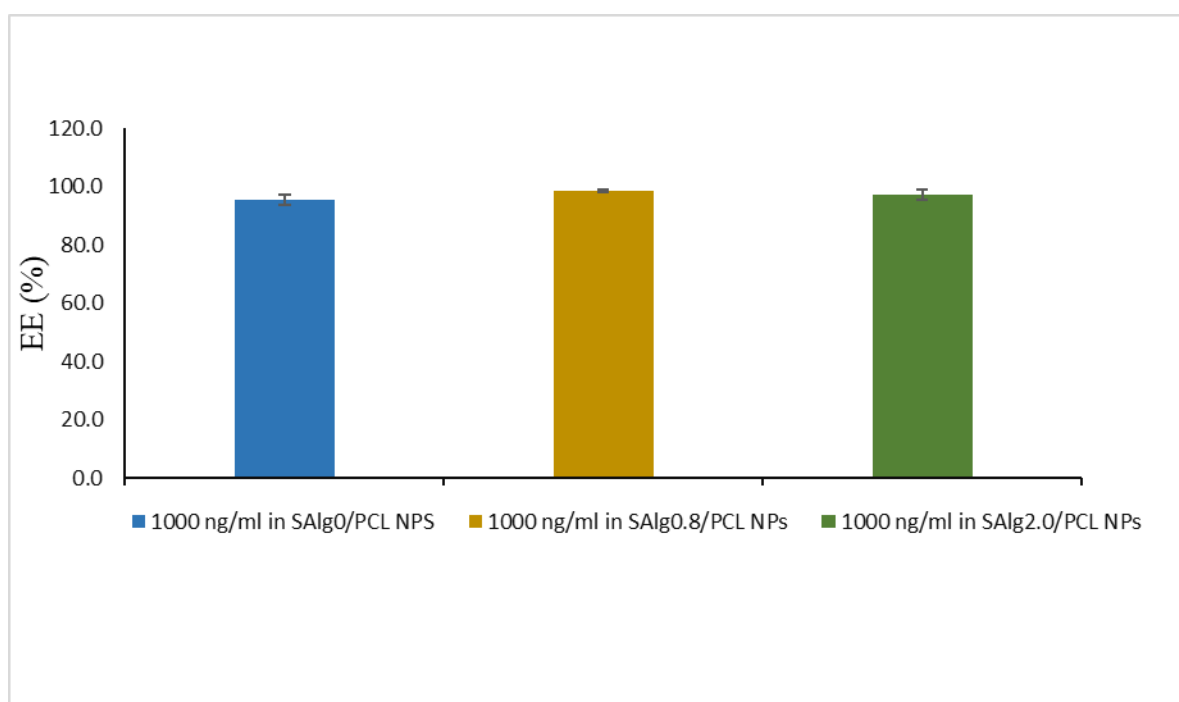


Figure 16. Encapsulation efficiency (EE %) of 1000 ng/ml of IGF-1 entrapped in AlgSulf₀, AlgSulf_{0.8}, and AlgSulf_{2.0}/PCL NPs. The data is reported as mean ± SEM (n=2).

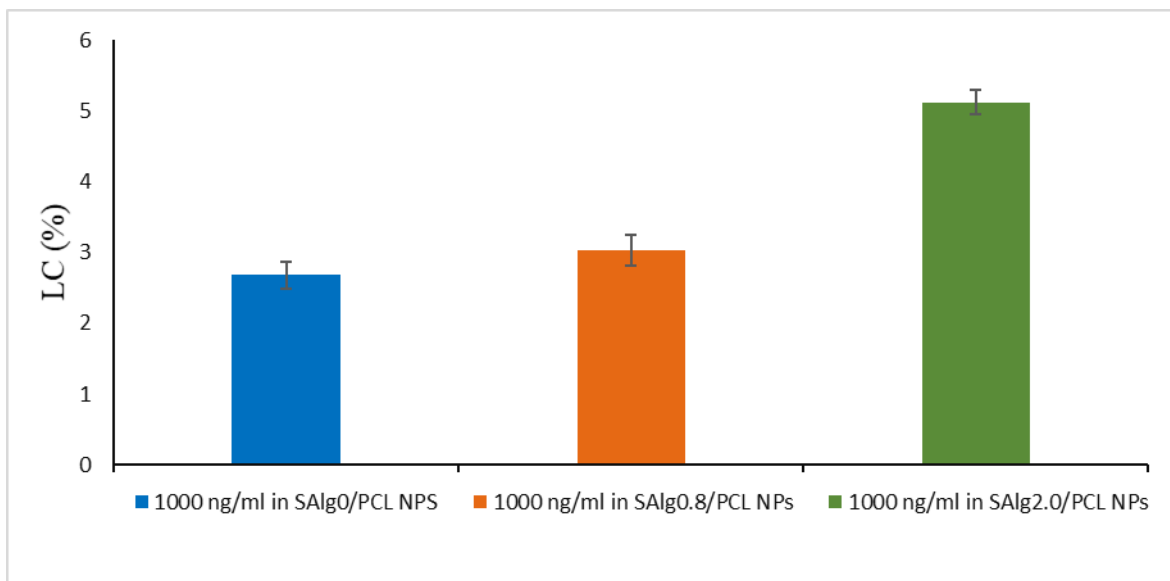


Figure 17. Loading capacity (%) of 1000 ng/ml of IGF-1 entrapped in AlgSulf₀, AlgSulf_{0.8}, and AlgSulf_{2.0}/PCL NPs. The data are presented as mean ± SEM (n=2).

5.3. In vitro Release Rate of IGF-1 from NPs

The *in vitro* cumulative release profile of IGF-1 from AlgSulf_{2.0}/PCL and AlgSulf_{0.0}/PCL NPs analyzed at 37°C as a function of time is shown in Fig.18. The IGF-1 drug release appears in a manner of two phases, an initial rapid burst release phase followed by a sustained release phase. About 18 % of the drug were released from AlgSulf_{0.0}/PCL NPs and about 7 % of the drug were released from AlgSulf_{2.0}/PCL NPs in the burst release phase within the first 2 hours, which was mainly due to the diffusion of IGF-1 that was absorbed on the NPs' surface instead of getting entrapped within the core. The sustained release phase takes place on a longer time interval since it happens as the drugs are released from the NPs due to the degradation of the polymers.

The release rate of IGF-1 from AlgSulf_{2.0}/PCL NPs was slower than that from AlgSulf_{0.0}/PCL NPs, which could be attributed to the heparin-mimetic characteristic of AlgSulf_{2.0} in the inner phase of the AlgSulf_{2.0}/PCL NPs which provides it with a higher binding affinity to heparin-binding GFs [44]. This higher binding affinity of the IGF-1 to the AlgSulf_{2.0} compared to AlgSulf_{0.0} in the inner aqueous phase of the AlgSulf_{2.0}/PCL NPs led to a decreased release rate of the IGF-1 compared to the AlgSulf_{0.0}/PCL NPs.

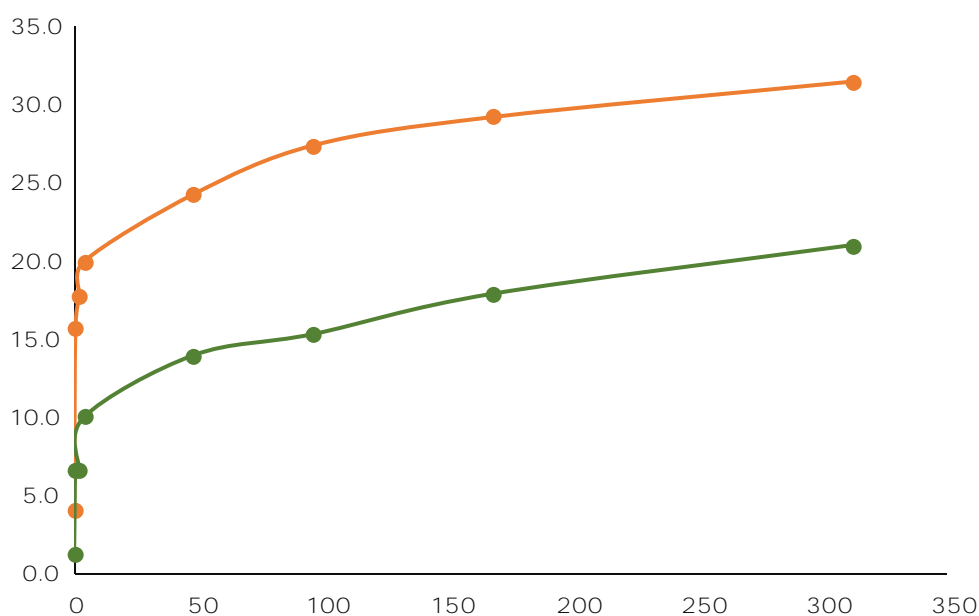


Figure 18. Cumulative release rate (%) of IGF-1 from AlgSulf₀/PCL and AlgSulf_{2.0}/PCL NPs. The data are presented as percentages (n=1).

5.4. Cytotoxicity Assessment

The toxic effects of the AlgSulf/PCL NPs were tested on HaCaT, a human keratinocytes cell line, through three different approaches including Trypan blue exclusion assay and MTT assay.

5.4.1. Trypan Blue Exclusion Assay

To study the effect of NPs on the viability of HaCaT cells, cells were treated with increasing concentrations of NPs (0, 5, 25, 50, 100 µg/ml) and Trypan blue exclusion assay was performed at 24-, 48-, and 72-hours post-treatment. The % viability of the cells reflects their ability to grow and recover in the presence of the mentioned concentrations of NPs. Here, the % viability was calculated using a formula that relates the number of dead cells to live ones in the well. After counting the number of dead and live cells in each well, the following formula was applied:

$\% \text{ viability} = \frac{\text{viable cells}}{(\text{dead cells} + \text{viable cells})} \times 100$. The two-way ANOVA test showed that the interaction parameter between concentration and time was not significant ($p=0.8002$) implying that the effect of the different concentrations of NPs on cell viability is independent of time. After 24 hours of incubation with NPs at concentrations of 50 and 100 µg/mL, a significant decrease in cell viability was observed compared to non-treated controls ($p<0.01$ and $p<0.0001$, respectively). Moreover, after 48 and 72 hours of incubation, cell viability decreased significantly only at the highest concentration of 100 µg/mL ($p<0.0001$) as evident in fig. 19.

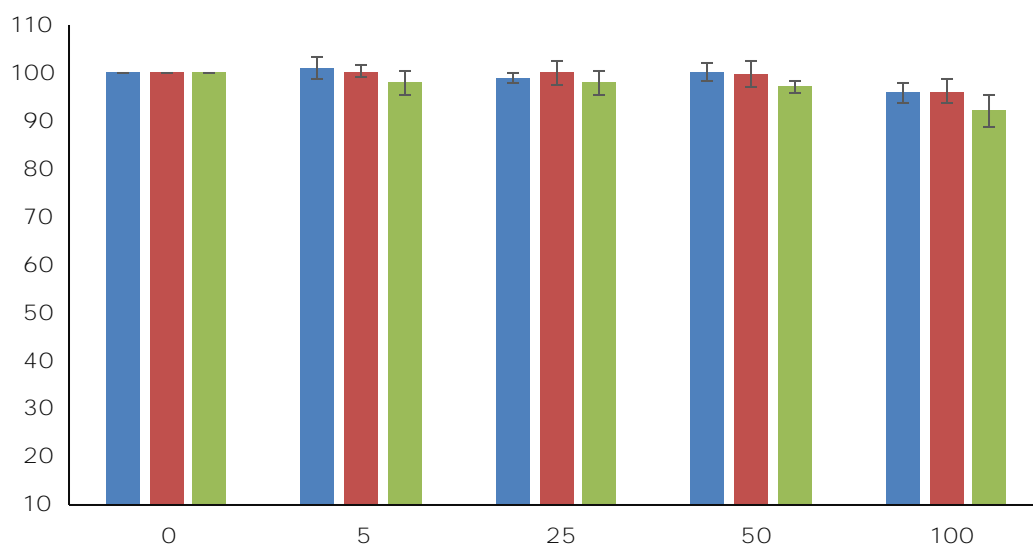


Figure 19. %Viability of HaCaT cells using Trypan Blue exclusion assay, n=3. The interaction parameter between concentration and time was not significant, p value=0.8002 as shown by two-way ANOVA test. Particle concentration was a significant factor ($p<0.0001$) where significant differences were found at 50 $\mu\text{g/mL}$ ($p<0.01$) at 24 hours and at 100 $\mu\text{g/mL}$ at all time-points ($p<0.0001$). However, no significant difference was found at any concentration after 24, 48, or 72 hours as time was not a significant factor ($p=0.1139$). Error bars include mean \pm SEM.

The % viability of AlgSulf_{0,0}/PCL NPs was previously evaluated at the same mentioned time-points and NPs' concentrations. The results showed that based on two-way ANOVA the interaction parameter between concentration of NPs and time was not significant ($p=0.165$). Moreover, at concentrations 50 and 100 $\mu\text{g/mL}$, there was a significant decrease with $p < 0.05$. At these two concentrations, the viability increased significantly after 72 hours indicating a decrease in viability with increased concentration (Supplementary Data Fig. S1). It is important to note however that AlgSulf_{2,0}/PCL NPs did not decrease cell viability below 83.46 % attained at 100 $\mu\text{g/mL}$ after 72 hours, suggesting only a mild toxic effect of HaCaT cells.

5.4.2. *MTT Assay*

Additionally, to study the effect of NPs on the metabolic activity of HaCaT cells, cells were treated with increasing concentrations of NPs and MTT assay was performed at the same time-points mentioned previously in 4.1. The concentrations of the NPs added were equivalent to the ones used in the Trypan blue assay relevant to the surface area of the wells.

As illustrated in fig. 20, NPs concentrations of 5, 25, 50, and 100 $\mu\text{g/ml}$ significantly decreased the cells' activity after a prolonged incubation of 72 hours as compared to non-treated controls ($p < 0.0001$). Moreover, the highest concentration of 100 $\mu\text{g/ml}$ significantly decreased cells' metabolic activity as early as 48 hours of incubation. Also, based on two-way ANOVA test, the interaction parameter between concentration and time was not significant ($p < 0.0001$) indicating that the effect of the different concentrations of NPs on cell activity is independent of time. We noticed that the cell viability determined by MTT was lower as compared to that determined by the Trypan blue assay. However, it is important to note here that the MTT assay does not specifically reflect the viability of the cells rather, it reflects their metabolic activity. MTT is based on the metabolic activity of the cells that is the amount of energy reflected by the number of mitochondria of cells suggesting that this decrease can be related to the normal cells weakening and degradation after a prolonged 72-hour period of time [100]. Also, the significant decrease in cell viability observed as early as 48 hours of incubation at 100 $\mu\text{g/ml}$ may be due to the excessive stress exerted on the cells

due to the high load of NPs rather than an actual toxic effect. Moreover, polymeric NPs mainly enter the cells by endocytosis, a process that is energy dependent. Thus, it is probable that the cells lost more energy during endocytosis as the concentration of NPs increased which further explains our results [105].

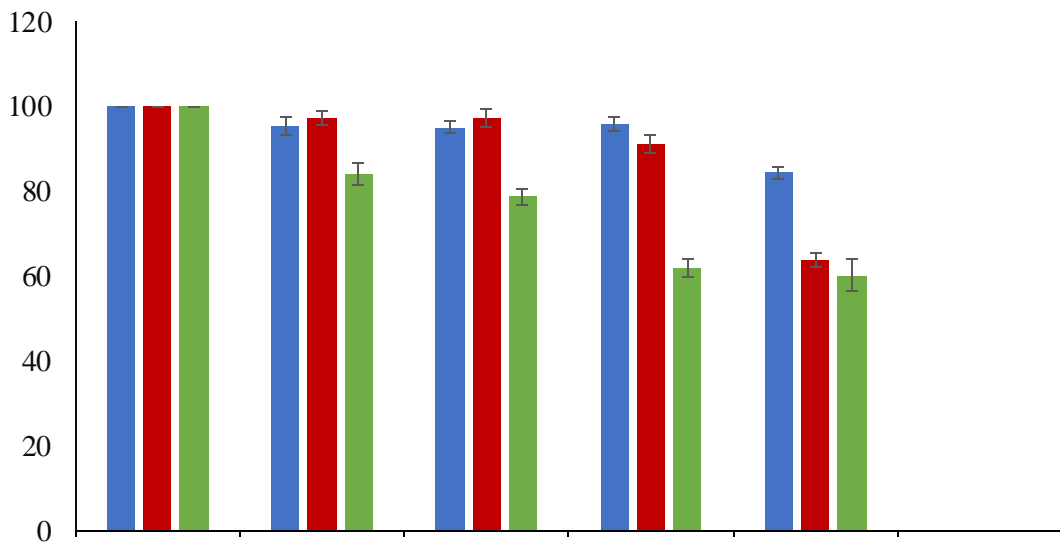


Figure 20. % Activity of HaCaT cells using MTT assay, n=3. The interaction parameter between concentration and time was significant with $p < 0.0001$ as shown by two-way ANOVA. Particle concentration was a significant factor ($p < 0.0001$) where significant differences were found at 100 $\mu\text{g/mL}$ after 48 hours ($p < 0.0001$) and at all concentrations after 72 hours ($p < 0.0001$). Time was also a significant factor ($p < 0.0001$) where significant differences were found at 24 hours for 100 $\mu\text{g/mL}$ ($p < 0.0001$), at 48 hours for 50 and 100 $\mu\text{g/mL}$ ($p < 0.01$ and $p < 0.0001$, respectively), and at 72 hours for all concentrations ($p < 0.0001$). Error bars include \pm SEM.

5.5. Cellular Uptake

To investigate the capacity of the synthesized NPs to penetrate cells, FITC-AlgSulf_{0.0}/PCL NPs and FITC-AlgSulf_{2.0}/PCL NPs were incubated with HaCaT cells at the concentration of 100 $\mu\text{g/mL}$ for 2, 4, and 24 hours. Then the fluorescence intensity

was measured by spectroscopy and the uptake efficiency calculated and presented in Fig 21. The particles' size was 235 nm and 395 nm, respectively. Similar pattern of uptake that was time dependent was observed for both types of NPs. Figure 21 shows that the percentage uptake of NPs by HaCaT cells was affected by the sulfation of alginates. The cellular uptake efficiency decreased from 17.72 ± 0.856 % for AlgSulf_{0,0}/PCL NPs to 14.95 ± 0.470 % for AlgSulf_{2,0}/PCL NPs at 2 hours, from 43.63 ± 0.211 % for AlgSulf_{0,0}/PCL NPs to 16.47 ± 0.154 % for AlgSulf_{2,0}/PCL NPs at 4 hours, and from 51.50 ± 0.851 % for AlgSulf_{0,0}/PCL NPs to 22.62 ± 1.397 % for AlgSulf_{2,0}/PCL NPs at 24 hours. It was shown that using AlgSulf_{2,0} instead of Alg in the NPs led to lower cellular uptake efficiency. The results also showed that cellular uptake efficiency increased with prolonged incubation time. Indeed, it increased sharply when incubation time changed from 2 to 4 hours in case of AlgSulf₀/PCL NPs. However, a milder change was observed when incubation time was prolonged to 24 hours. This suggests that when time was extended to 4 hours, the concentration of NPs inside the cells got close to the cellular uptake threshold.

The cellular uptake of polymeric NPs most often takes place through endocytosis, a process that consists of two steps, binding to cellular membrane and internalization. The first step is affected by the physicochemical properties of the NPs, mainly their surface charge. A possible reason for the decrease in HaCaT cellular uptake when it comes to AlgSulf_{2,0}/PCL NPs as compared AlgSulf_{0,0}/PCL NPs is that AlgSulf_{2,0} is more negatively charged when compared to pure Alg. AlgSulf_{2,0} has sulfate groups that are more negatively charged than carboxyl groups present in pure Alg [46]. Thus, the more negative the surface charge of the NPs, the more the electrostatic

repulsion takes place between the negatively charged NPs and the negatively charged cellular membrane, leading to reduced number of internalized NPs [102, 103].

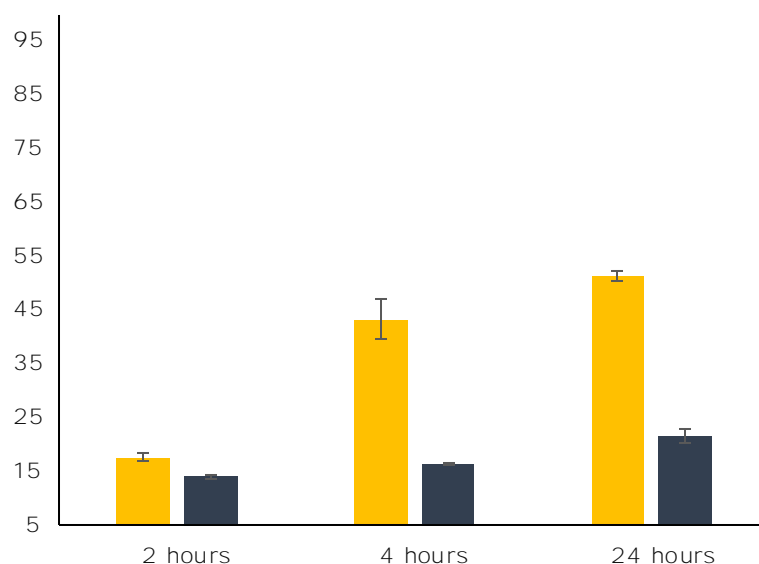


Figure 21. Cellular Uptake Efficiency (%) of Alg/PCL NPs and AlgSulf_{2.0}/PCL NPs by HaCaT cells. $p=0.0094$ as shown by one-way ANOVA for FITC-AlgSulf_{0.0}/PCL NPs. Tukey post hoc's test shows significant difference ($*p<0.05$) between 2 and 4 hours, and between 2 and 24 hours. For FITC-AlgSulf_{2.0}/PCL NPs, $p=0.0112$ as shown by one-way ANOVA. Tukey post hoc's test shows significant difference ($*p<0.05$) between 2 and 24 hours and 4 hours, and between 2 and 24 hours. All samples were synthesized as $n=3$ and error bars include \pm SEM.

Whilst the cellular uptake efficiency of AlgSulf_{2.0}/PCL NPs is less than that of AlgSulf_{0.0}/PCL NPs with time, it is important to take into consideration that the toxicity profile of AlgSulf_{0.0}/PCL NPs increases starting 50 $\mu\text{g/mL}$ at 24 hours compared to the toxicity profile of AlgSulf_{2.0}/PCL NPs that remains insignificant up to 72 hours according to the trypan blue assay. Thus, the decrease in cellular uptake for AlgSulf_{2.0}/PCL NPs is advantageous because the lower the number of internalized NPs, the lower the exerted stress, thus, the lower the toxicity. Also, IGF-1 is a GF that works at the ECM to initiate the repairing process and prepare the wound bed to the

inflammatory stage of the wound healing phases. Thus, it is favorable for IGF-1 to be released from the NPs outside the cell [33].

5.6. AlgSulf-coated Alg/PCL NPs Synthesis and Characterization

The characteristics of the synthesized NPs based on the average size, zeta potential, and PDI are presented in table 5. The NPs had an average size of 292 ± 14.96 nm, with PDI value less than 0.3. Small sized NPs are known to have a better interaction with cells compared to larger particles with size > 500 nm [104]. Furthermore, SEM images of the NPs supported more information regarding the morphology of the NPs. Figure 22 shows that the NPs have a smooth spherical shape.

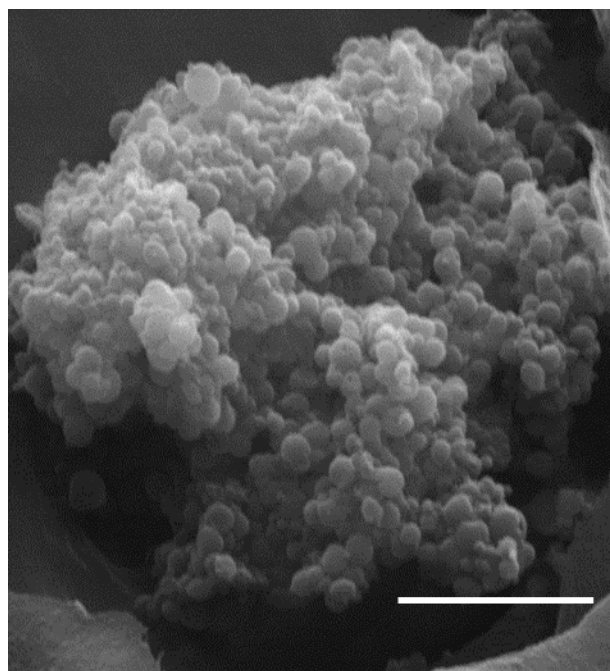


Figure 22. SEM image of AlgSulf-coated Alg/PCL NPs. Scale bar = 5 μ m.

Regarding the surface charge, the particles presented a negative zeta potential value as expected due to the AlgSulf on their outer surface being negatively charged. As compared to Alg/PCL NPs that had -11.1 mV, the AlgSulf_{2,0}-coated Alg/PCL NPs had a

more negative zeta potential value of -19 ± 1.9 mV due to the presence of the negatively charged AlgSulf on the outer phase.

Sample	Average Size (nm)	Zeta Potential (mV)	PDI
AlgSulf-coated Alg/PCL NPs	292.017 ± 14.96	-19.39 ± 1.9	0.167 ± 0.03

Table 5. Size, Zeta Potential, and PDI of AlgSulf-coated Alg/PCL NPs. Results are present as mean \pm SEM (n=2).

Identification of AlgSulf-coated Alg/PCL NPs constituents

To further confirm the presence of the AlgSulf_{2.0} outer coating phase on the NPs, they were analyzed using FTIR spectrophotometer for characteristic absorption bands to study the functional groups present in the sample. Figure 23 shows a specific sharp PCL peak at 1750 cm^{-1} for the AlgSulf_{2.0}-coated Alg/PCL NPs. In fact, Alg ideally shows a weak peak at 1415 cm^{-1} due to the symmetric and asymmetric stretching of carboxyl groups of alginates[106]. The AlgSulf_{2.0} and AlgSulf_{2.0}-coated Alg/PCL NPs also exhibit a sharp peak at 1250 cm^{-1} assigned to the S=O asymmetric stretching indicating the sulfation of Alg as well as a minor peak at 800 cm^{-1} corresponding to S–O–C stretching, and peak at 3400 cm^{-1} indicating stretching vibration of O-H groups. Those peaks refer to the sulfation of uronic acids in pure Alg. Moreover, the multiple peaks observed between $1549 - 1053\text{ cm}^{-1}$ refers to the presence of semi-crystalline synthetic polymer PVA [106, 107].

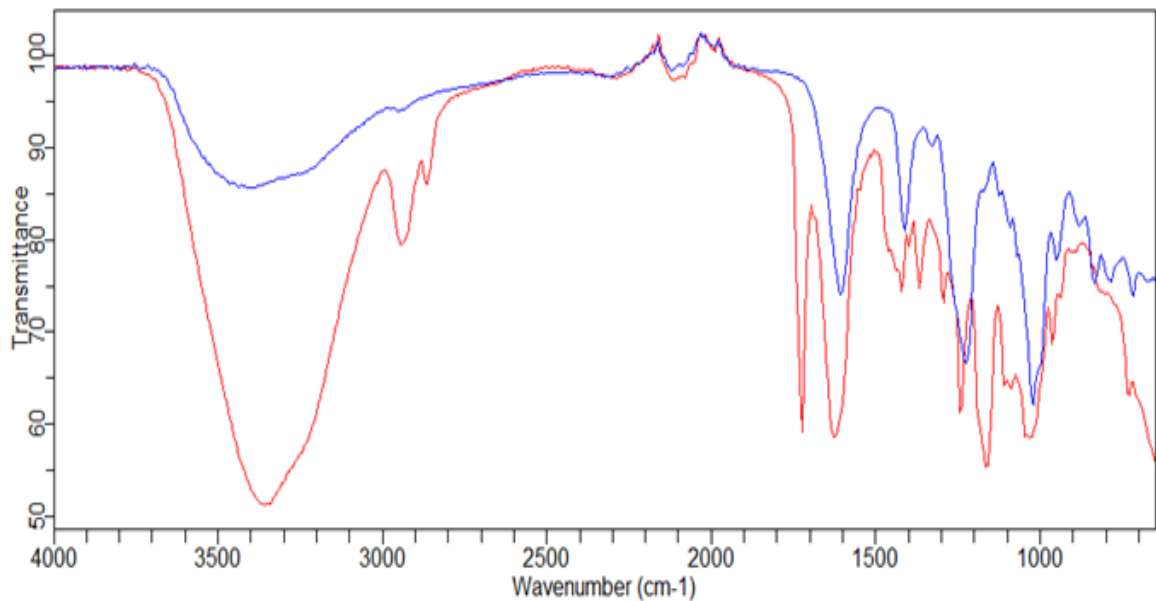


Figure 23. FTIR Spectrum of AlgSulf-coated Alg/PCL NPs. The blue spectrum represents that of AlgSulf_{2.0} alone, and the red spectrum represents that of AlgSulf_{2.0}-coated Alg/PCL NPs.

5.7. AlgSulf-coated Alg/PCL NPs effect on inflammatory cytokines

We assessed whether the AlgSulf_{2.0}-coated Alg/PCL NPs could reduce the inflammatory cytokines typically present in the wound microenvironment. Accordingly, HaCaT cells were cultured in a high glucose medium to mimic diabetic conditions, and treated with lipopolysaccharide (LPS) to induce inflammation. They were then treated with Alg, AlgSulf, IGF-1, Alg/PCL NPs, AlgSulf_{2.0}/PCL NPs, AlgSulf_{2.0}-coated Alg/PCL NPs, as well as IGF-1 loaded NPs to evaluate their effect on the inflammatory cytokine IL-6. Figure 24 shows that Alg/PCL NPs, AlgSulf_{2.0}/PCL NPs, AlgSulf_{2.0}-coated Alg/PCL NPs led to a decrease in human IL-6 gene expression compared to the LPS (+ve) treated control. Importantly, the AlgSulf_{2.0}-coated Alg/PCL NPs led to a decrease in the expression of hIL-6 around 2-folds when compared to the positive control. The hIL-6 expression decreased in all treatments compared to the positive

control. When treating cells with IGF-1 loaded NPs, a similar trend to bare NPs was shown. IGF-1 loaded Alg/PCL NPs lead to a decrease in hIL-6 expression followed by a further decrease by IGF-1 loaded AlgSulf_{2.0}/PCL and IGF-1 loaded AlgSulf_{2.0}-coated Alg/PCL NPs, respectively. Comparing the IGF-1 loaded NPs to the bare NPs, the cells treated with IGF-1 loaded AlgSulf_{2.0}-coated Alg/PCL NPs expressed a lower amount of hIL-6 compared to cells treated with bare AlgSulf-coated Alg/PCL NPs.

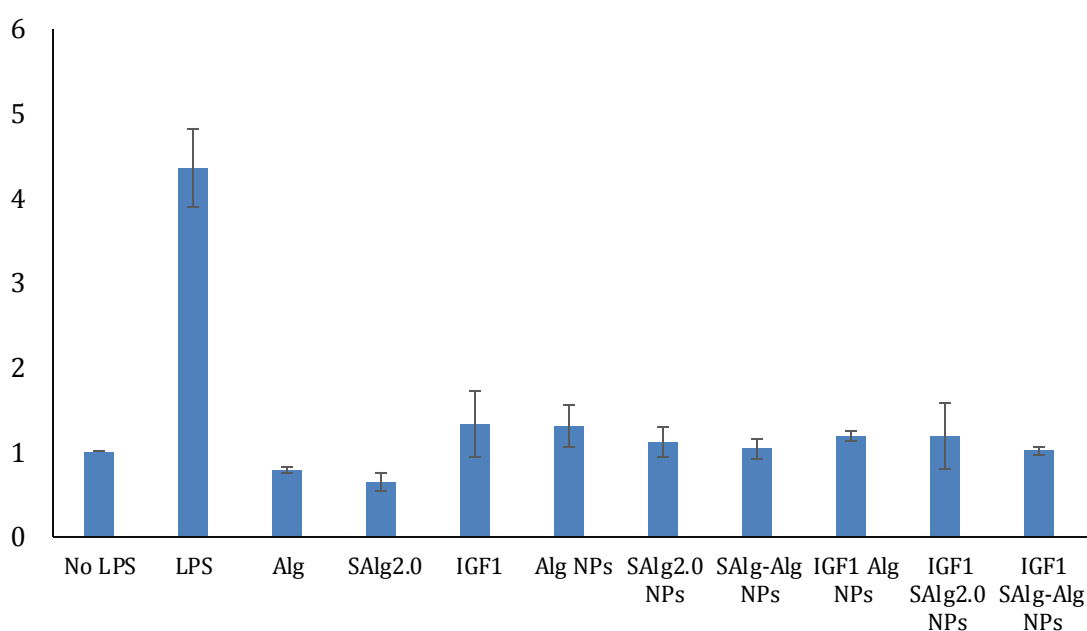


Figure 24. mRNA expression of hIL-6 in HaCaT cells after 24 hours of inducing inflammation by LPS and treating the cells with Alg, AlgSulf, IGF-1, Alg/PCL NPs, AlgSulf_{2.0}/PCL NPs, AlgSulf_{2.0}-coated Alg/PCL NPs, and IGF-1 loaded NPs. The data are present as mean ± SEM (n=2).

To confirm the ability of the NPs to bind and sequester IL-6, we performed an ELISA assay to measure released hIL-6 proteins in the supernatant of all the 11 conditions. Figure 25 shows similar results to those shown in Figure 24, where the supernatant of AlgSulf_{2.0}-coated Alg/PCL NPs treated cells showed less amount of hIL-

6 in the media compared to Alg/PCL NPs and AlgSulf_{2.0}/PCL NPs. Also, the supernatant of IGF-1 loaded AlgSulf_{2.0}-coated Alg/PCL NPs treated cells showed less amount of hIL-6 released compared to the supernatant of cells treated with IGF-1 loaded Alg/PCL NPs and IGF-1 loaded AlgSulf_{2.0}/PCL NPs. The amount of IL-6 present in the supernatant of cells treated with free AlgSulf_{2.0} was, as expected, less than that in the supernatant of cells treated with pure Alg and that is due to the higher ability of AlgSulf_{2.0} to bind to IL-6. Also, IGF-1 is known to exhibit anti-inflammatory activities when delivered at low concentrations [108]. IGF-1 and IGF-1 loaded NPs lead to a decrease in the IL-6 levels as shown in both figures 24 and 25. The supernatant of cells treated with IGF-loaded AlgSulf_{2.0}-coated Alg/PCL NPs showed a decrease in the IL-6 amount released by cells.

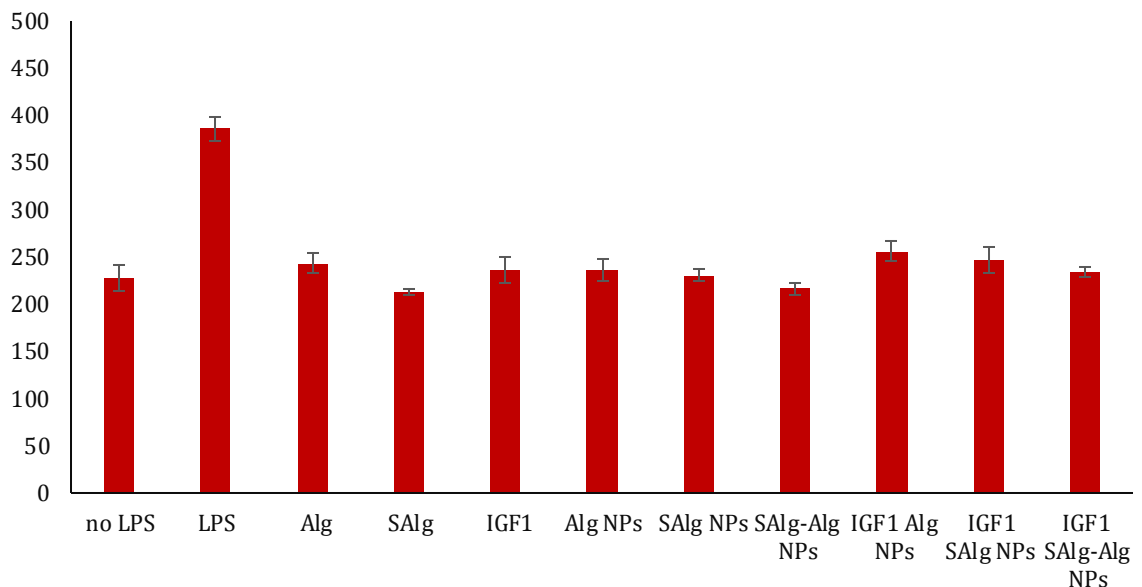


Figure 25. Amount of hIL-6 released by HaCaT cells into the supernatant after 24 hours of inducing inflammation by LPS and treating the cells with Alg, AlgSulf, IGF-1, Alg/PCL NPs, AlgSulf_{2.0}/PCL NPs, AlgSulf_{2.0}-coated Alg/PCL NPs, and IGF-1 loaded NPs. The data are present as mean \pm SEM (n=2).

These results show an increased role of the NPs with AlgSulf_{2.0} coating or in the inner phase in decreasing levels of IL-6 pro-inflammation cytokine due to the sequestration effect of AlgSulf_{2.0} on the outer coating that is shown by ELISA assay after collecting the supernatants along with the PCR results. AlgSulf_{2.0} represents a heparin/heparan sulfate analogue not only for it associates with heparin-binding GFs, but also because it promotes the sequestration of inflammatory proteins. It was proposed by a previous study that AlgSulf_{2.0} possess their anti-inflammatory properties through sequestration and binding to inflammatory mediators, such as IL-1b and IL-6 [46]. This revealed a vital role of GAG-mimicking AlgSulf that could be an advantage for medical drug delivery uses.

CHAPTER 6

CONCLUSION

DFU is a cause of chronic wound conditions that, if healed, takes a prolonged period that is painful to the patient. There is an increasing need to accelerate the wound healing process in these conditions to prevent major complications of non-healed DFU such as limbs' gangrenes that further lead to amputations. The deficiency in GFs and anti-inflammatory markers have a major destructive role on the normal orchestrating multi-step wound healing process in diabetic patients. IGF-1 is one of the essential GFs that become deficient at the wound site in DFU, and can be administered to enhance the healing process. GFs, including IGF-1, have a short half-life and thus need to be administered continuously at high doses. To overcome the obstacle of short half-life, a lot of research is being invested in the synthesis of controlled drug delivery systems that have the required physicochemical properties and characteristics in terms of biocompatibility, biodegradability, surface charge, hydrodynamic size, among others. Alg, AlgSulf, PCL, and PVA are biocompatible, FDA approved, and widely available polysaccharides, that are used in drug delivery and medical applications. In this project, we synthesized Alg/PCL, AlgSulf/PCL, and AlgSulf-coated Alg/PCL NPs using the double emulsion solvent evaporation technique to be able to control and adjust the size, zeta-potential, morphology, drug encapsulation efficiency, and drug release rate properties of the NPs. The size, zeta potential, PDI, and morphology of the NPs were studied under the condition of different DS of Alg. The NPs were also loaded with IGF-1 and the encapsulation efficiency, loading capacity, and release rate were analyzed. Both, AlgSulf/PCL and Alg/PCL NPs presented high desired encapsulation efficiency

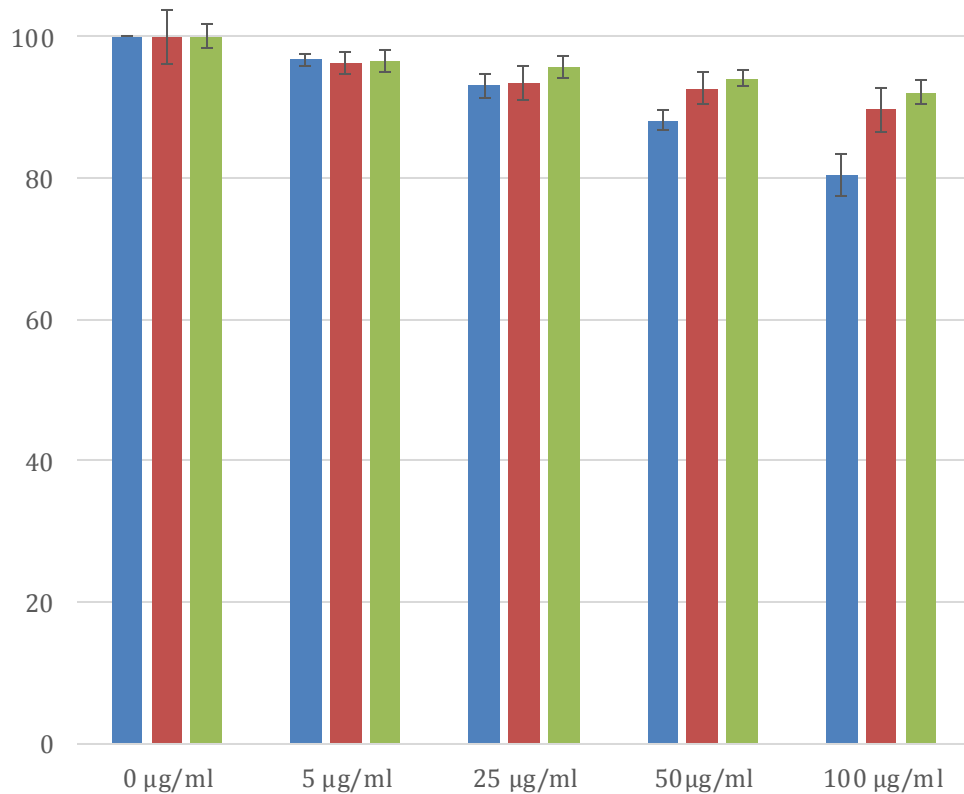
of IGF-1, also AlgSulf/PCL NPs showed a slower release rate of IGF-1 as a function of time compared to Alg/PCL NPs. Regarding the cytotoxicity studies, the trypan blue exclusion assay as function of time shows that the NPs maintained a relatively high viability of HaCaT cells and did not exhibit major toxic effects. AlgSulf presents scavenging properties by which it binds to free inflammatory marker proteins such as IL-6 and IL-1b. Thus, to present a drug delivery system with dual activity, Alg/PCL NPs were coated with AlgSulf.

In summary, we have engineered and characterized a novel DDS of polymeric NPs comprising Alg and AlgSulf, demonstrated its biocompatibility, its ability to entrap and release IGF-1 in a slow and sustained manner, as well as shown its dual ability to sequester inflammatory proteins to promote faster wound repair. This DDS will be further tested for its ability to promote migration of wounded keratinocytes and induce wound closure along with decreasing the inflammatory cytokines in the media using a scratch assay.

In the future, this system can be tested on *in vivo* DFU models to validate its ability to promote wound repair. The NPs can be applied either directly on the wound area, or within a scaffold that could be made of biocompatible Alg. This novel DDS can also be utilized to entrap other types of hydrophobic and/or hydrophilic drugs especially those with heparin-binding affinity for different biomedical applications.

APPENDIX

Supplementary Data



Supplementary Data Figure 1. % Viability of HaCaT cells using Trypan Blue as a
h w p e v k q p " q h " P R The interaction parameter between concentration and time was not significant $P=0.165$ as shown by a Two-Way ANOVA, particle concentration was a significant factor $P<0.05$ with significant differences for concentrations $\geq 25\mu\text{g/ml}$ (# non-significant compared to $0\mu\text{g/ml}$). However, for 72h cultures significant differences were only found at $100\mu\text{g/ml}$ as show by One-Way Anova $*P<0.05$, and for 24h cultures significant differences were found at 50 and $100\mu\text{g/ml}$. The data is reported as mean \pm SEM (n=3).

REFERENCES

1. Yazdanpanah, L., M. Nasiri, and S. Adarvishi, *Literature review on the management of diabetic foot ulcer*. World journal of diabetes, 2015. **6**(1): p. 37.
2. Lotfy, M., et al., *Chronic complications of diabetes mellitus: a mini review*. Current diabetes reviews, 2017. **13**(1): p. 3-10.
3. Daneman, D., *Type 1 diabetes*. The Lancet, 2006. **367**(9513): p. 847-858.
4. Stirban, A., P. Rösen, and D. Tschoepe, *Complications of type 1 diabetes: new molecular findings*. Mount Sinai Journal of Medicine: A Journal of Translational and Personalized Medicine: A Journal of Translational and Personalized Medicine, 2008. **75**(4): p. 328-351.
5. Schmidt, A.M., *Highlighting diabetes mellitus: The epidemic continues*. Arteriosclerosis, thrombosis, and vascular biology, 2018. **38**(1): p. e1-e8.
6. Mhanna, R., et al., *Sulfated alginate as a mimic of sulfated glycosaminoglycans: binding of growth factors and effect on stem cell behavior*. Advanced Biosystems, 2017. **1**(7): p. 1700043.
7. Iqbal, M., et al., *Preparation of biodegradable PCL particles via double emulsion evaporation method using ultrasound technique*. Colloid and Polymer Science, 2015. **293**(3): p. 861-873.
8. Baker, M.I., et al., *A review of polyvinyl alcohol and its uses in cartilage and orthopedic applications*. Journal of Biomedical Materials Research Part B: Applied Biomaterials, 2012. **100**(5): p. 1451-1457.
9. Mordorski, B. and T. Prow, *Nanomaterials for wound healing*. Current Dermatology Reports, 2016. **5**(4): p. 278-286.
10. Moura, L.I., et al., *Recent advances on the development of wound dressings for diabetic foot ulcer treatment ô a review*. Acta biomaterialia, 2013. **9**(7): p. 7093-7114.
11. Salsali, A. and M. Nathan, *A review of types 1 and 2 diabetes mellitus and their treatment with insulin*. American journal of therapeutics, 2006. **13**(4): p. 349-361.
12. Vehik, K. and D. Dabelea, *The changing epidemiology of type 1 diabetes: why is it going through the roof?* Diabetes/metabolism research and reviews, 2011. **27**(1): p. 3-13.
13. Whiting, D.R., et al., *IDF diabetes atlas: global estimates of the prevalence of diabetes for 2011 and 2030*. Diabetes research and clinical practice, 2011. **94**(3): p. 311-321.
14. Leahy, J.L., *Pathogenesis of type 2 diabetes mellitus*. Archives of medical research, 2005. **36**(3): p. 197-209.
15. Wang, J., et al., *Dietary energy density predicts the risk of incident type 2 diabetes: the European Prospective Investigation of Cancer (EPIC)-Norfolk Study*. Diabetes Care, 2008. **31**(11): p. 2120-2125.
16. Alfadhli, E.M., *Gestational diabetes mellitus*. Saudi medical journal, 2015. **36**(4): p. 399.
17. Fowler, M.J., *Microvascular and macrovascular complications of diabetes*. Clinical diabetes, 2011. **29**(3): p. 116-122.
18. Harding, J.L., et al., *Global trends in diabetes complications: a review of current evidence*. Diabetologia, 2019. **62**(1): p. 3-16.

19. Armstrong, D.G., A.J. Boulton, and S.A. Bus, *Diabetic foot ulcers and their recurrence*. New England Journal of Medicine, 2017. **376**(24): p. 2367-2375.
20. de Smet, G.H., et al., *Oxygen therapies and their effects on wound healing*. Wound Repair and Regeneration, 2017. **25**(4): p. 591-608.
21. Lim, J.Z.M., N.S.L. Ng, and C. Thomas, *Prevention and treatment of diabetic foot ulcers*. Journal of the Royal Society of Medicine, 2017. **110**(3): p. 104-109.
22. Oyibo, S.O., et al., *A comparison of two diabetic foot ulcer classification systems: the Wagner and the University of Texas wound classification systems*. Diabetes care, 2001. **24**(1): p. 84-88.
23. Enoch, S. and D.J. Leaper, *Basic science of wound healing*. Surgery (Oxford), 2005. **23**(2): p. 37-42.
24. da Silva, L., E. Carvalho, and M.T. Cruz, *Role of neuropeptides in skin inflammation and its involvement in diabetic wound healing*. Expert opinion on biological therapy, 2010. **10**(10): p. 1427-1439.
25. Rathur, H. and A. Boulton, *Recent advances in the diagnosis and management of diabetic neuropathy*. The Journal of bone and joint surgery. British volume, 2005. **87**(12): p. 1605-1610.
26. Yan, W., et al., *Acellular dermal matrix scaffolds coated with connective tissue growth factor accelerate diabetic wound healing by increasing fibronectin through PKC signalling pathway*. Journal of Tissue Engineering and Regenerative Medicine, 2018. **12**(3): p. e1461-e1473.
27. Henshaw, F.R., et al., *Topically applied connective tissue growth factor/CCN2 improves diabetic preclinical cutaneous wound healing: potential role for CTGF in human diabetic foot ulcer healing*. Journal of diabetes research, 2015. **2015**.
28. Olczyk, P., Ł. Mencner, and K. Komosinska-Vassev, *The role of the extracellular matrix components in cutaneous wound healing*. BioMed research international, 2014. **2014**.
29. Higginson, J.R., et al., *Differential sulfation remodelling of heparan sulfate by extracellular 6-O-sulfatases regulates fibroblast growth factor-induced boundary formation by glial cells: implications for glial cell transplantation*. Journal of Neuroscience, 2012. **32**(45): p. 15902-15912.
30. Lyon, M., G. Rushton, and J.T. Gallagher, *The interaction of the transforming growth factor- β 1 with heparan sulfate*. Journal of Biological Chemistry, 1997. **272**(29): p. 18000-18006.
31. Rider, C., *Heparin/heparan sulphate binding in the TGF- β 1 signaling pathway*. 2006, Portland Press Ltd.
32. Brem, H. and M. Tomic-Canic, *Cellular and molecular basis of wound healing in diabetes*. The Journal of clinical investigation, 2007. **117**(5): p. 1219-1222.
33. Ghatak, S., et al., *Roles of proteoglycans and glycosaminoglycans in wound healing and fibrosis*. International journal of cell biology, 2015. **2015**.
34. Sarrazin, S., W.C. Lamanna, and J.D. Esko, *Heparan sulfate proteoglycans*. Cold Spring Harbor perspectives in biology, 2011. **3**(7): p. a004952.
35. Freedman, M.D., *Pharmacodynamics, clinical indications, and adverse effects of heparin*. The Journal of Clinical Pharmacology, 1992. **32**(7): p. 584-596.
36. Christman, K.L., et al., *Nanoscale growth factor patterns by immobilization on a heparin-mimicking polymer*. Journal of the American Chemical Society, 2008. **130**(49): p. 16585-16591.

37. Mousavi, S., et al, *Anti-inflammatory effects of heparin and its derivatives: a systematic review*. Advances in pharmacological sciences, 2015. **2015**.
38. Blakytny, R., et al, *Lack of insulin-like growth factor 1 (IGF1) in the basal keratinocyte layer of diabetic skin and diabetic foot ulcers*. J Pathol, 2000. **190**(5): p. 589-94.
39. Aydin, F., et al, *IGF-I Increases with Hyperbaric Oxygen Therapy and Promotes Wound Healing in Diabetic Foot Ulcers*. J Diabetes Res, 2013. **2013**: p. 567834.
40. Laron, Z., *Insulin-like growth factor 1 (IGF-1): a growth hormone*. Mol Pathol, 2001. **54**(5): p. 311-6.
41. Botusan, I.R., et al, *Deficiency of liver-derived insulin-like growth factor-I (IGF-I) does not interfere with the skin wound healing rate*. PLoS One, 2018. **13**(3): p. e0193084.
42. Sjögren, K., et al, *Liver-derived insulin-like growth factor I (IGF-I) is the principal source of IGF-I in blood but is not required for postnatal body growth in mice*. Proc Natl Acad Sci U S A, 1999. **96**(12): p. 7088-92.
43. Igarashi, A., et al, *Regulation of connective tissue growth factor gene expression in human skin fibroblasts and during wound repair*. Mol Biol Cell, 1993. **4**(6): p. 637-45.
44. Freeman, I., A. Kedem, and S. Cohen, *The effect of sulfation of alginate hydrogels on the specific binding and controlled release of heparin-binding proteins*. Biomaterials, 2008. **29**(22): p. 3260-3268.
45. Barrientos, S., et al, *Growth factors and cytokines in wound healing*. Wound Repair Regen, 2008. **16**(5): p. 585-601.
46. Arlov, Ø., et al, *Biomimetic sulphated alginate hydrogels suppress IL-1B-induced inflammatory responses in human chondrocytes*. 2017.
47. Dinh, T., et al, *Mechanisms involved in the development and healing of diabetic foot ulceration*. Diabetes, 2012. **61**(11): p. 2937-47.
48. Xu, F., C. Zhang, and D.T. Graves, *Abnormal cell responses and role of TNF- α in impaired diabetic wound healing*. Biomed Res Int, 2013. **2013**: p. 754802.
49. Kantae, V., et al, *Integration of pharmacometabolomics with pharmacokinetics and pharmacodynamics: towards personalized drug therapy*. Metabolomics, 2017. **13**(1): p. 9.
50. Pridgen, E.M., F. Alexis, and O.C. Farokhzad, *Polymeric nanoparticle drug delivery technologies for oral delivery applications*. Expert Opin Drug Deliv, 2015. **12**(9): p. 1459-73.
51. Lewitt, M.S. and G.W. Boyd, *The Role of Insulin-Like Growth Factors and Insulin-Like Growth Factor-Binding Proteins in the Nervous System*. Biochem Insights, 2019. **12**: p. 1178626419842176.
52. Kotov, N.A., *Chemistry. Inorganic nanoparticles as protein mimics*. Science, 2010. **330**(6001): p. 188-9.
53. Min, Y., et al, *Clinical Translation of Nanomedicine*. Chem Rev, 2015. **115**(19): p. 11147-90.
54. Akbarzadeh, A., et al, *Liposome: classification, preparation, and applications*. Nanoscale Res Lett, 2013. **8**(1): p. 102.
55. Alavi, M., N. Karimi, and M. Safaei, *Application of Various Types of Liposomes in Drug Delivery Systems*. Adv Pharm Bull, 2017. **7**(1): p. 3-9.

56. Samad, A., Y. Sultana, and M. Aqil, *Liposomal drug delivery systems: an update review*. *Curr Drug Deliv*, 2007. **4**(4): p. 297-305.
57. Brandl, M., *Liposomes as drug carriers: a technological approach*. *Biotechnol Annu Rev*, 2001. **7**: p. 59-85.
58. Torchilin, V.P., *Structure and design of polymeric surfactant-based drug delivery systems*. *J Control Release*, 2001. **73**(2-3): p. 137-72.
59. Aliabadi, H.M. and A. Lavasanifar, *Polymeric micelles for drug delivery*. *Expert Opin Drug Deliv*, 2006. **3**(1): p. 139-62.
60. Gong, J., et al., *Polymeric micelles drug delivery system in oncology*. *J Control Release*, 2012. **159**(3): p. 312-23.
61. Yokoyama, M., *Polymeric micelles as drug carriers: their lights and shadows*. *J Drug Target*, 2014. **22**(7): p. 576-83.
62. Lu, Y., et al., *Micelles with ultralow critical micelle concentration as carriers for drug delivery*. *Nature biomedical engineering*, 2018. **2**(5): p. 318-325.
63. Naahidi, S., et al., *Biocompatibility of engineered nanoparticles for drug delivery*. *J Control Release*, 2013. **166**(2): p. 182-94.
64. Ranjan, S., et al., *Microparticles to enhance delivery of drugs and growth factors into wound sites*. *Ther Deliv*, 2016. **7**(10): p. 711-732.
65. Akbari, B., M.P. Tavandashti, and M. Zandrahimi, *Particle size characterization of nanoparticles á practical approach*. *Iranian Journal of Materials Science and Engineering*, 2011. **8**(2): p. 48-56.
66. Xue, M., et al., *Delivery systems of current biologicals for the treatment of chronic cutaneous wounds and severe burns*. *Advanced drug delivery reviews*, 2018. **129**: p. 219-241.
67. Kumari, A., S.K. Yadav, and S.C. Yadav, *Biodegradable polymeric nanoparticles based drug delivery systems*. *Colloids and surfaces B: biointerfaces*, 2010. **75**(1): p. 1-18.
68. Mokhtarzadeh, A., et al., *Recent advances on biocompatible and biodegradable nanoparticles as gene carriers*. *Expert opinion on biological therapy*, 2016. **16**(6): p. 771-785.
69. Liu, Z., et al., *Polysaccharides-based nanoparticles as drug delivery systems*. *Advanced drug delivery reviews*, 2008. **60**(15): p. 1650-1662.
70. Francis, R., N. Joy, and A. Sivadas, *Relevance of natural degradable polymers in the biomedical field*. *Bio-based Plastics–Materials and Applications*, 2017.
71. Jarai, B.M., et al., *Polymeric Nanoparticles*, in *Nanoparticles for Biomedical Applications*. 2020, Elsevier. p. 303-324.
72. Uchegbu, I.F., et al., *Fundamentals of pharmaceutical nanoscience*. 2013: Springer.
73. Gainza, G., et al., *rhEGF-loaded PLGA-Alginate microspheres enhance the healing of full-thickness excisional wounds in diabetised Wistar rats*. *European Journal of Pharmaceutical Sciences*, 2013. **50**(3-4): p. 243-252.
74. Gainza, G., et al., *Advances in drug delivery systems (DDSs) to release growth factors for wound healing and skin regeneration*. *Nanomedicine: Nanotechnology, Biology and Medicine*, 2015. **11**(6): p. 1551-1573.
75. Khalid, M. and H.S. El-Sawy, *Polymeric nanoparticles: promising platform for drug delivery*. *International journal of pharmaceutics*, 2017. **528**(1-2): p. 675-691.

76. Soppimath, K.S., et al., *Biodegradable polymeric nanoparticles as drug delivery devices*. Journal of controlled release, 2001. **70**(1-2): p. 1-20.
77. Gharieh, A., S. Khoei, and A.R. Mahdavian, *Emulsion and miniemulsion techniques in preparation of polymer nanoparticles with versatile characteristics*. Advances in colloid and interface science, 2019. **269**: p. 152-186.
78. Jenjob, R., et al., *Emulsion techniques for the production of pharmacological nanoparticles*. Macromolecular bioscience, 2019. **19**(6): p. 1900063.
79. Halima, N.B., *Poly (vinyl alcohol): review of its promising applications and insights into biodegradation*. RSC advances, 2016. **6**(46): p. 39823-39832.
80. Afshar, M., et al., *Preparation and characterization of sodium alginate/polyvinyl alcohol hydrogel containing drug-loaded chitosan nanoparticles as a drug delivery system*. Journal of Drug Delivery Science and Technology, 2020. **56**: p. 101530.
81. Hajiali, F., S. Tajbakhsh, and A. Shojaei, *Fabrication and properties of polycaprolactone composites containing calcium phosphate-based ceramics and bioactive glasses in bone tissue engineering: a review*. Polymer reviews, 2018. **58**(1): p. 164-207.
82. Puppi, D., et al., *Polymeric materials for bone and cartilage repair*. Progress in polymer Science, 2010. **35**(4): p. 403-440.
83. Ansary, R.H., M.B. Awang, and M.M. Rahman, *Biodegradable poly (D, L-lactic-co-glycolic acid)-based micro/nanoparticles for sustained release of protein drugs-A review*. Tropical Journal of Pharmaceutical Research, 2014. **13**(7): p. 1179-1190.
84. Walter, E., et al., *Hydrophilic poly (DL-lactide-co-glycolide) microspheres for the delivery of DNA to human-derived macrophages and dendritic cells*. Journal of Controlled Release, 2001. **76**(1-2): p. 149-168.
85. Tønnesen, H.H. and J. Karlsen, *Alginate in drug delivery systems*. Drug development and industrial pharmacy, 2002. **28**(6): p. 621-630.
86. Lee, K.Y. and D.J. Mooney, *Alginate: properties and biomedical applications*. Progress in polymer science, 2012. **37**(1): p. 106-126.
87. Jain, D. and D. Bar-Shalom, *Alginate drug delivery systems: application in context of pharmaceutical and biomedical research*. Drug development and industrial pharmacy, 2014. **40**(12): p. 1576-1584.
88. Boateng, J.S., et al., *Wound healing dressings and drug delivery systems: a review*. Journal of pharmaceutical sciences, 2008. **97**(8): p. 2892-2923.
89. Mhanna, R., et al., *Chondrocyte culture in three dimensional alginate sulfate hydrogels promotes proliferation while maintaining expression of chondrogenic markers*. Tissue Engineering Part A, 2014. **20**(9-10): p. 1454-1464.
90. Arlov, Ø. and G. Skjåk-Bræk, *Sulfated alginates as heparin analogues: a review of chemical and functional properties*. Molecules, 2017. **22**(5): p. 778.
91. Zhang, Z. and S.-S. Feng, *The drug encapsulation efficiency, in vitro drug release, cellular uptake and cytotoxicity of paclitaxel-loaded poly (lactide) δ tocopheryl polyethylene glycol succinate nanoparticles*. Biomaterials, 2006. **27**(21): p. 4025-4033.
92. Canton, I. and G. Battaglia, *Endocytosis at the nanoscale*. Chemical Society Reviews, 2012. **41**(7): p. 2718-2739.

93. Siqueira, P.-C., et al., *Cytotoxicity of glass ionomer cements containing silver nanoparticles*. Journal of clinical and experimental dentistry, 2015. **7**(5): p. e622.
94. Kong, B., et al., *Experimental considerations on the cytotoxicity of nanoparticles*. Nanomedicine, 2011. **6**(5): p. 929-941.
95. Fried, J.R., *Polymer science and technology*. 2014: Pearson Education.
96. Silveira, N., et al., *Synthesis and characterization of the antitubercular phenazine lapazine and development of PLGA and PCL nanoparticles for its entrapment*. Materials Science and Engineering: C, 2016. **58**: p. 458-466.
97. Kulkarni, S.A. and S.-S. Feng, *Effects of particle size and surface modification on cellular uptake and biodistribution of polymeric nanoparticles for drug delivery*. Pharmaceutical research, 2013. **30**(10): p. 2512-2522.
98. Zakeri-Milani, P., et al., *The characteristics and improved intestinal permeability of vancomycin PLGA-nanoparticles as colloidal drug delivery system*. Colloids and Surfaces B: Biointerfaces, 2013. **103**: p. 174-181.
99. Bhattacharjee, S., *DLS and zeta potential ówhat they are and what they are not?* Journal of controlled release, 2016. **235**: p. 337-351.
100. He, C., et al., *Effects of particle size and surface charge on cellular uptake and biodistribution of polymeric nanoparticles*. Biomaterials, 2010. **31**(13): p. 3657-3666.
101. Mark, H.F., *Encyclopedia of polymer science and technology, 15 volume set*. Vol. 14. 2014: Wiley New York, NY, USA:.
102. Patil, S., et al., *Protein adsorption and cellular uptake of cerium oxide nanoparticles as a function of zeta potential*. Biomaterials, 2007. **28**(31): p. 4600-4607.
103. Oh, N. and J.-H. Park, *Endocytosis and exocytosis of nanoparticles in mammalian cells*. International journal of nanomedicine, 2014. **9**(Suppl 1): p. 51.
104. Florence, A.T., *The oral absorption of micro-and nanoparticulates: neither exceptional nor unusual*. Pharmaceutical research, 1997. **14**(3): p. 259-266.
105. Panariti, A., G. Miserocchi, and I. Rivolta, *The effect of nanoparticle uptake on cellular behavior: disrupting or enabling functions?* Nanotechnology, science and applications, 2012. **5**: p. 87.
106. Hu, W.-W., Y.-C. Wu, and Z.-C. Hu, *The development of an alginate/polycaprolactone composite scaffold for in situ transfection application*. Carbohydrate polymers, 2018. **183**: p. 29-36.
107. Silverstein, R.M. and G.C. Bassler, *Spectrometric identification of organic compounds*. Journal of Chemical Education, 1962. **39**(11): p. 546.
108. Mangiola, A., et al., *Role and importance of IGF-1 in traumatic brain injuries*. BioMed research international, 2015. **2015**.

